Emilie Bruand, C. Storey, M. Fowler

HAL Id: hal-02347260
https://hal.science/hal-02347260

Submitted on 5 Nov 2019

Accessory Mineral Chemistry of High Ba–Sr Granites from Northern Scotland: Constraints on Petrogenesis and Records of Whole-rock Signature

E. BRUAND*, C. STOREY AND M. FOWLER

SCHOOL OF EARTH AND ENVIRONMENTAL SCIENCES, UNIVERSITY OF PORTSMOUTH, BURNABY BUILDING, BURNABY ROAD, PORTSMOUTH PO1 3QL, UK

The Rogart and Strontian high Ba–Sr plutons (Northern Highlands, Scotland) comprise a range of lithologies from felsic to ultramafic rocks. The latter are mantle-derived and their differentiation to produce the felsic components of the plutons is the result of fractional crystallization and variable assimilation of the surrounding Moine metasediments. New results presented here demonstrate that accessory mineral chemistry can provide further insight into their petrogenesis and highlight the petrological potential of apatite and titanite. The main accessory minerals titanite, apatite and zircon contain most of the rare earth elements (REE) in the high Ba–Sr plutons. Results for apatite and titanite show that careful imaging and in situ trace element analysis provide constraints on the petrogenetic history of the host-rock. In both plutons, apatite and titanite record in situ crystallization and fractionation. In Strontian, both apatite and titanite from the granitoids record a mixing event with mafic magma in their rim compositions. Apatite and titanite chemistries are sensitive to the nature of their host-rocks (felsic versus ultramafic) and some elements (e.g. Sr, V) closely reflect whole-rock chemistry and the degree of fractionation. In some cases, whole-rock trace element concentrations can be calculated based on accessory mineral chemistry. Thus, trace elements in accessory minerals can give direct access to the nature and crystallization history of plutonic rocks. This petrological tool may be helpful in provenance studies using accessory minerals, and because high Ba–Sr plutons have recently been equated with Archaean sanukitoids, this might also be important in constraining the temporal distribution of this important magma type.

INTRODUCTION

The Strontian and Rogart plutons are typical high Ba–Sr granites in that they have high Ba–Sr contents, are extremely rich in light rare earth elements (LREE) and have relatively low Nb, Ta, and heavy rare earth element (HREE) abundances. They have been discussed in the literature for their high modal abundance of accessory minerals (mainly titanite and apatite, with lesser zircon and monazite; e.g. Paterson *et al.*, 1989; Paterson & Stephens, 1992). Their whole-rock chemistry and isotope systematics (O, Nd and Sr) argue for a mantle-derived parent magma modified by fractional crystallization and host metasediment assimilation (Fowler *et al.*, 2008). Although the whole-rock chemistry (trace element, radiogenic and stable isotopes) of the Rogart and Strontian plutons is well constrained (Fowler *et al.*, 2001, 2008), studies of accessory minerals in other intrusions have demonstrated that these can give additional information on petrogenesis (e.g. Sha & Chappell, 1999; Hoskin *et al.*, 2000; Tiepolo *et al.*, 2002). The incorporation of trace elements and more particularly rare earth elements (REE) into their structures makes them ideal minerals for this purpose. More specifically, previous studies concentrating on titanite and apatite have suggested that these minerals might be sensitive to

* Corresponding author. E-mail: emilie.bruand@port.ac.uk

mixing processes, $f\mathrm{O}_2$, fluid circulation or P–T conditions (e.g. Tepper & Kuehner, 1999; Piccoli *et al.*, 2000; Belousova *et al.*, 2002*a*; Smith *et al.*, 2009; McLeod *et al.*, 2011). Recent work also shows promise in linking apatite compositions to their host-rocks (Chu *et al.*, 2009; Belousova *et al.*, 2002*a*; Jennings *et al.*, 2011). On the other hand, although zircon is a well-known accessory phase with many geological applications, its utility as a petrogenetic tracer is still not fully understood (e.g. Hoskin *et al.*, 2000; Hoskin & Schaltegger, 2003; Gagnevin *et al.*, 2010). Although most studies focus on describing one of the accessory minerals contained within a suite of rocks (e.g. Sha & Chappell, 1999; Tepper & Kuehner, 1999; Piccoli *et al.*, 2000; Belousova *et al.*, 2002*a*; McLeod *et al.*, 2011), comparison of the various accessory minerals within a suite of samples has been rarely done (Hoskin *et al.*, 2000). As they all contain REE, systematic comparative studies are essential to understand their behaviour in different conditions. In this contribution, we study apatite, titanite and zircon in a suite of rocks from the Strontian and Rogart high Ba–Sr granites and develop a new petrographic tool to understand the behaviour of these phases in a range of felsic to mafic intrusive igneous rocks.

Recent advances in mineral trace element chemistry may also be exploited for sedimentary provenance studies and to constrain crustal evolution. Similarities between high Ba–Sr granites and sanukitoids have led previous workers to describe them as 'Phanerozoic sanukitoids' (Fowler & Rollinson, 2012). Sanukitoids are interpreted as being the products of partial melting of a metasomatized mantle wedge and have been reported as occurring during a short geological time span ($\sim$2·7–2·5 Ga; Martin *et al.*, 2009). They have been interpreted by various workers (e.g. Martin *et al.*, 2009) as the result of changes from a shallow to a steep subduction style in this time interval and therefore might mark the onset of modern plate tectonics. Given this potentially pivotal role, it is important to constrain their temporal distribution. Assuming that accessory minerals record the geochemical characteristics of their host magmas, it should be possible to recognize different igneous protoliths in detrital heavy mineral assemblages. For example, if the high Ba–Sr (sanukitoid) 'fingerprint' is shown to be robust, then it can be sought in representative sediments of different ages, to monitor changing sanukitoid abundance with time.

This study presents detailed petrographic observations and systematic laser ablation inductively coupled plasma mass spectrometry (LA-ICP-MS) analysis of trace elements in apatite, titanite and zircon, with two main aims: to better constrain the petrogenesis of high Ba–Sr granites, and to test the assumption that their characteristic chemistry is recorded by the abundant accessory minerals that they contain.

GEOLOGICAL SETTING AND SAMPLES
## Late Caledonian high Ba–Sr plutons
The late Caledonian orogeny in Scotland is marked by voluminous granite magmatism, resulting from the collision between Laurentia, Baltica and Avalonia following the closure of the Iapetus Ocean during Silurian times (Soper *et al.*, 1992; Atherton & Ghani, 2002). The plutons have a broadly calc-alkaline composition and are widespread within the Scottish Highlands north of the Iapetus Suture (Soper, 1986; Fig. 1). Three suites have been distinguished (Stephens & Halliday, 1984): the Argyll suite (now modified to the Argyll and Northern Highlands suite; Stephenson *et al.*, 1999), the Cairngorm suite and the South of Scotland suite. Most plutons of the last suite have now been subsumed into the Trans-Suture suite (Brown *et al.*, 2008). High Ba–Sr granites (Tarney & Jones, 1994) characterize the Argyll and Northern Highlands suite and are the particular focus of this contribution. Their origin has previously been ascribed to slab break-off (Atherton & Ghani, 2002; Fowler *et al.*, 2008).

In the Northern Highlands, the Caledonian foreland is separated from Moine Supergroup metasediments, into which the high Ba–Sr plutons were emplaced, by the Moine Thrust. To the south, the Great Glen Fault defines the boundary between the Northern Highland Terrane and the Grampian Terrane. The Midland Valley and Southern Uplands define the southern part of the Scottish Highlands between the Grampian Highlands and the Iapetus Suture.

The late Caledonian high Ba–Sr suite intruding the Northern Highland terrane can be divided petrographically into two groups: (1) a western area dominated by syenitic plutons and (2) a central–eastern area dominated by granitic plutons (e.g. Fowler *et al.*, 2008, and references therein). We present data obtained from single mineral grains (titanite, apatite, zircon) from the Rogart and Strontian plutons; these are both granite-dominated igneous complexes from the central–eastern area (Fig. 1).

Rogart and Strontian igneous complexes
The Rogart and Strontian igneous complexes have a broadly concentric geometry and are mainly made up of biotite–hornblende granodiorite. Emplacement of the Strontian complex caused contact metamorphism evidenced by cordierite–K feldspar and sillimanite–K feldspar mineral assemblages in the adjacent country rocks (Soper, 1963; Tyler & Ashworth, 1983); no contact metamorphism is observed around the Rogart pluton. Strontian has a biotite granodiorite central facies surrounded by hornblende–biotite granodiorite, which grades from porphyritic to non-porphyritic at its margin (Sabine, 1963). The hornblende–biotite granodiorite has been dated at 425 ± 3 Ma (U–Pb on zircon) and 423 ± 3 Ma (U–Pb
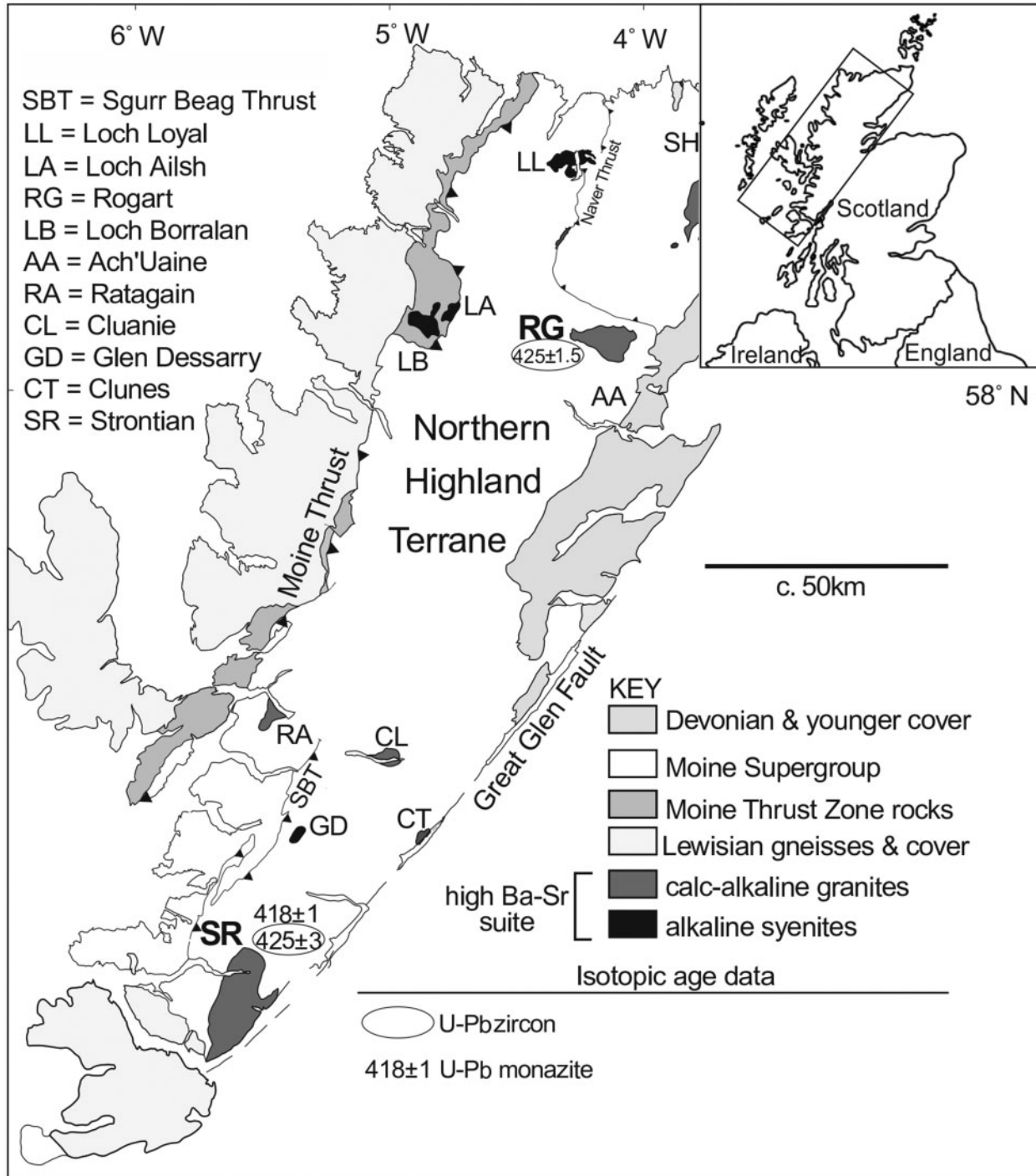
Fig. 1. Map of the Northern Highland region (Scotland) modified after Fowler *et al.* (2008), showing sample localities and ages (in Ma) from Brown *et al.* (1968) and Rogers & Dunning (1991).

on titanite; Rogers & Dunning, 1991). The Rogart igneous complex is made up of an inner granodiorite and an outer tonalite, both of which are cross-cut by a later granite. It is contemporaneous with Strontian and has been dated at around 420 Ma (K–Ar on biotite; Brown *et al.*, 1968) and

425 ±1·5 Ma (U–Pb on zircon; Kocks *et al.*, 2013). Mafic igneous bodies (from centimetres to hundreds of metres in scale), referred to as appinites, were first described from the Appin area by Bailey & Maufe (1916) and are present in the main facies of both the Strontian and Rogart

plutonic bodies. Appinites are mantle-derived rocks with shoshonitic affinities (Fowler, 1988; Fowler *et al.*, 2008), and are widely believed to be the plutonic equivalents of calc-alkaline lamprophyres (Rock, 1984; Murphy, 2013). Their high Mg, Ni, Cr and V contents indicate a mantle source component in their petrogenesis. In these rocks, hornblende is the dominant mafic mineral and occurs mainly as large prismatic crystals contained in a groundmass of hornblende and feldspar ± quartz. Local mingling and mixing relationships are observed between the main plutonic facies and the appinite bodies, especially at Strontian. The Strontian pluton was derived from a depleted mantle source and Rogart from an enriched mantle source, as discussed in detail by Fowler *et al.* (2008). Both plutons evolved by fractional crystallization and variable assimilation of the surrounding Moine metasediments.

In this contribution, seven samples in total have been studied: two hornblende–biotite granodiorites (SR1, SR3) and one appinite (SR2) from Strontian, and two tonalites (RT1, R2), one granite (RHG-1) and one appinite (RA1) from Rogart. All samples from both plutons contain abundant accessory minerals such as titanite, apatite and zircon and are exceptional in that respect (Table 1). The hb–bi granodiorite samples from Strontian are chemically similar with SiO_2 ranging from 62·81 to 63·83% (Fowler *et al.*, 2008) and an Aluminium Saturation Index [ASI, calculated as molecular: $Al_2O_3/(Na_2O + K_2O + CaO)$] ranging from 0·87 to 0·90. Overall their trace element contents are also similar and have been described in detail by Fowler *et al.* (2008). Granitoid compositions from Rogart vary extensively (Fowler *et al.*, 2001). In Rogart, tonalites vary in SiO_2 between 62·98 and 71·20%, Fe_2O_3 between 2·78 and 4·71% and their ASI are 0·81 (RT1) and 0·91 (R2). The granitic sample (RHG-1) has a somewhat comparable chemistry in major elements to R2 with an ASI of 0·92 but with slightly higher K_2O and CaO contents (Fowler *et al.*, 2001). Trace element contents vary significantly between the Rogart samples [e.g. Sr ranges from 693 ppm (RHG-1) to 1333 ppm (RT1); see Fowler *et al.* (2001) for analyses]. In the tonalitic samples, RT1 has higher contents of Cr, Ni and Nb compared with R2, which can be linked to less fractionation, following Fowler *et al.* (2001).

Appinites in the central–eastern Northern Highlands carry the high Ba–Sr geochemical signature, but are commonly even more enriched in large ion lithophile elements (LILE; e.g. Sr, Ba), high field strength elements (HFSE; e.g. Nb, Th) and transition metals (e.g. Cr, Ni, V) than the associated granodiorites and granites (Fowler *et al.*, 2008). These characteristics can be observed in the two appinitic samples studied here (SR2 and RA1). However, some compositional differences do exist between them. In terms of major elements, the Strontian appinite is richer in Fe_2O_3 but has a higher ASI (0·59, compared with Rogart ASI = 0·49). The sample from Rogart is more enriched in Sr, Ba and LREE compared with that from Strontian, but has lower HREE, Zr, Cr and Ni.

ANALYTICAL METHODS
Image acquisition
The samples were crushed (jaw-crusher, ball mill or Selfrag^TM), sieved (<355 µm, 355–500 µm and 500–1000 µm fractions) and passed over a Wilfley table. A diamagnetic separator was then used to obtain fractions of different heavy minerals based on their diamagnetic properties. Titanite, apatite and zircon were handpicked, mounted in epoxy resin discs and polished for *in situ* chemical analysis. Titanite and apatite were also analysed

Table 1: Estimated modal proportion of titanite, apatite and zircon in the Rogart and Strontian samples

Sample	Rock type	Grid reference	Mineralogy	Titanite(%)*	Apatite(%)*	Zircon(%)*
Strontian						
SR1	Granodiorite	NM795611	hbl–fsp–bt–qz	2–3	1	<1
SR2	Appinite	NM786611	hbl–fsp–bt ± cc	5	1–2	<0·5
SR3	Granodiorite	NM779607	hbl–fsp–bt–qz ± aln	1–2	<1	<1
Rogart						
RHG-1	Granite	NC671046	fsp–bt–qz ± chl–cal	1–2	1–2	<1
R2	Tonalite	NC709029	hbl–fsp–qz–bt–ms ± aln	1	<1	<1
RT1	Tonalite	NC741065	hbl–fsp–qz–bt–ms ± aln	1–2	1	<1
RA1	Appinite	NC702026	hbl–cpx–fsp–bt ± cc	3	5	<0·3

The grid reference system used is the Ordnance Survey National Grid reference system using OSGB 36 datum. Mineral abbreviations are after Whitney & Evans (2010).
*Modal proportion.

within thick sections (*c.* 150 μm). Back-scattered electron (BSE) images of titanites were taken with a scanning electron microscope (SEM) JEOL JSM-6100 at the University of Portsmouth (accelerating voltage = 20 kV). Cathodoluminescence (CL) images of apatites and zircons were taken with a KeDev Centaurus CL detector housed on a JEOL 6060LV SEM also at the University of Portsmouth (accelerating voltage = 15 kV).

Electron probe microanalysis (EPMA)

A Cameca SX-100 microprobe at Bristol University was used for determination of major elements in titanite and zircon using TAP, LPET, PET and LLIF crystals. PC0, TAP, LPET and LLIF crystals were used for apatite. An electron beam of 1 μm was used for titanite and 10 μm for apatite, both with 20 kV accelerating voltage and 40 nA and 10 nA beam currents, respectively. An electron beam of 5 μm was used for zircon with an accelerating voltage of 17 kV and a beam current of 100 nA. Several trace elements in these minerals were also analysed for comparison with LA-ICP-MS data. The Durango apatite standard (Marks *et al.*, 2012) and the 91500 zircon standard (Wiedenbeck *et al.*, 2004) were analysed during microprobe sessions to monitor data quality.

Laser ablation-inductively coupled plasma mass spectrometry (LA-ICP-MS)

Trace element contents of titanite, apatite and zircon were analysed by LA-ICP-MS at the University of Portsmouth using an Agilent 7500cs (quadrupole) ICP-MS system and a New-Wave UP213 (λ = 213 nm) solid-state Nd:YAG laser. Each analysis consisted of *c.* 30 s background acquisition and 60 s sample acquisition. The diameter of the laser beam was 30 μm for titanite and apatite and either 30 μm or 40 μm for zircon (with a 10 Hz repetition rate, an output energy of 0·01–0·1 mJ per pulse, and a fluence of ~4 J cm^{-2}). Each analytical run had either nine or 16 spot analyses with at least two external standard analyses at the beginning and end of each run (either NIST 610 or NIST 612). NIST 610 standard (Pearce *et al.*, 1997) was analysed with a laser beam diameter of 55 μm before and after titanite and apatite unknown runs. In addition, Durango apatite (reference value used: Marks *et al.*, 2012) was also analysed with a laser beam diameter of 30 μm at the beginning of each apatite run. NIST 612 standard (Pearce *et al.*, 1997) was analysed before and after zircon unknown runs with a laser beam diameter of 55 μm. The 91500 standard was analysed (Wiedenbeck *et al.*, 2004) with a beam diameter of 40 μm at the beginning of each zircon run. Details of the standard analyses and their comparison with literature data can be found in the Supplementary Data Electronic Electronic Appendix 1 (supplementary data are available at http://www.petrology.oxfordjournals.org). Internal references used for normalization of LA-ICP-MS data were ^{43}Ca for apatite

and titanite, and ^{29}Si for zircon and were obtained by EPMA.

PETROGRAPHY

The hb–bi granodiorite samples from Strontian (SR1-SR3) mainly comprise hornblende, feldspar and biotite. Both samples contain titanite, apatite and zircon (Table 1) ± allanite. The two tonalite samples from Rogart (R2 and RT1) comprise biotite, feldspar, hornblende and muscovite. Accessory phases present in these samples are titanite, apatite and zircon ± allanite. The granite sample from Rogart (RHG-1) is mainly made up of partly sericitized feldspar and biotite, which is often replaced by chlorite and calcite. This sample is therefore more affected by alteration than the others considered in this study. Titanite, apatite and zircon are present.

Appinitic samples from both locations (SR2 and RA1) are mainly made up of hornblende, biotite and feldspar ± calcite. Sample RA1 contains pyroxene, which is fractured and often partially replaced by calcite, in contrast to SR2. Paterson *et al.* (1989) highlighted the exceptional amount of titanite in these rocks (Table 1), which also contain a large amount of apatite, together with minor zircon and allanite.

Titanite, apatite and zircon, occurring in every sample, are the focus of this study and their characteristics within the samples studied are described in the following section. Accessory allanite is occasionally observed in Rogart (R2 and RT1 samples) and less so in Strontian. Allanite is not a ubiquitous mineral across the range of samples analysed and is therefore not considered in this study.

Titanite

Bi–hb granodiorite: samples SR1and SR3

Titanites are euhedral and large (up to ~1 cm in length; Fig. 2). In BSE images at least three zones, grading from a bright core towards a dark rim, can be identified (Fig. 2a and b). Occasionally a thin (~10–40 μm), darker outer rim is present (Fig. 2a). The bright core often shows fir-tree zoning but also some oscillatory zoning, both of which are characteristic of titanite crystals (e.g. Paterson & Stephens, 1992; Watson & Liang, 1995; Hayden *et al.*, 2008; McLeod *et al.*, 2011; Fig. 2a and b). Locally, rare dissolution–reprecipitation textures have been identified. Apatite, Fe–Ti oxides and zircon occur as inclusions within titanite cores and rims.

Granite: sample RHG-1

Two generations of titanite can be identified on the basis of size and petrographic relationship with the rock-forming minerals. Large titanites (>500 μm in length) are euhedral, often replaced by oxides and/or calcite and are also found as inclusions in feldspar. Smaller titanites (<500 μm in length) are subhedral, locally replaced by chlorite and
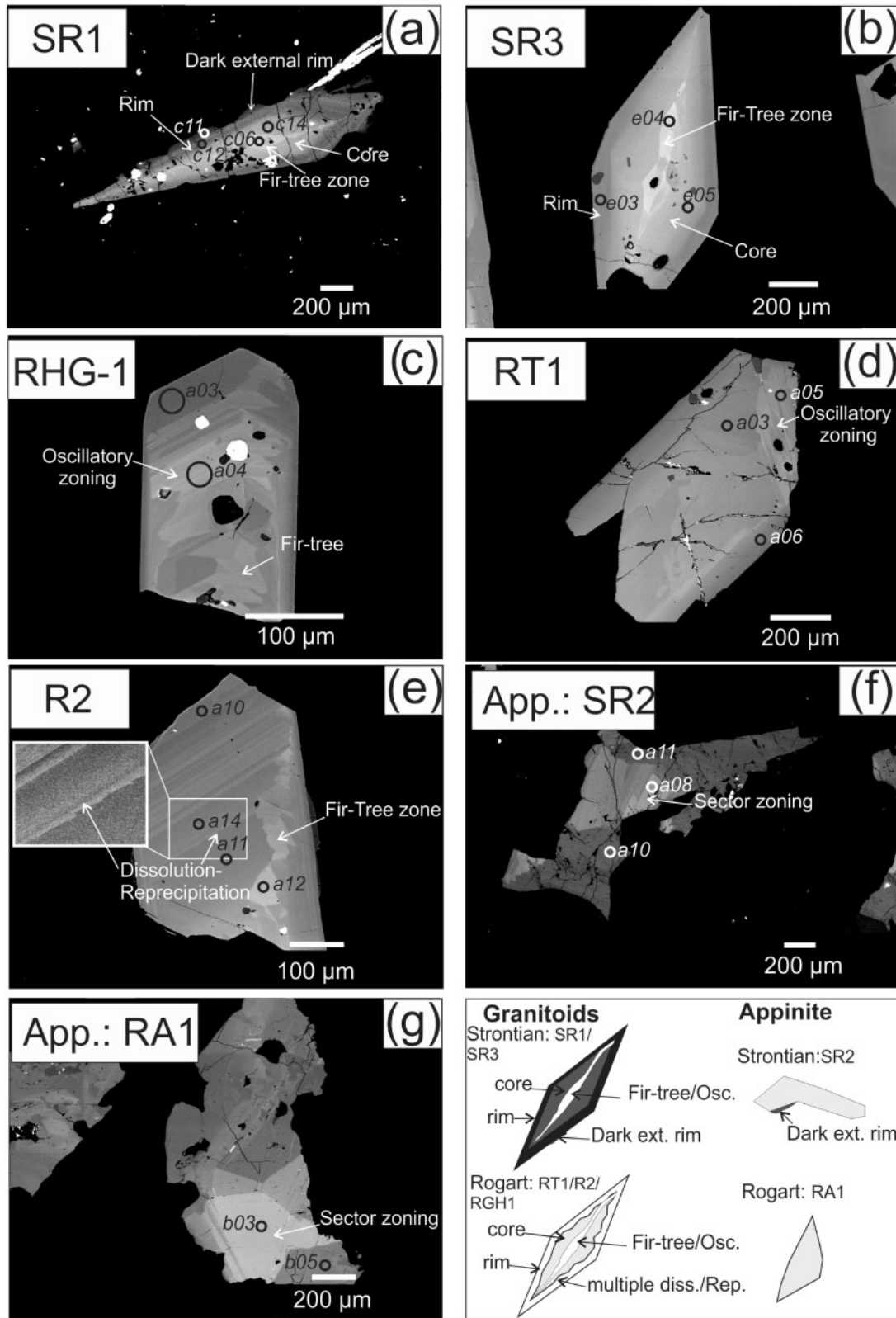
Fig. 2. Back-scattered electron images of titanite crystals from the Strontian (a, b, f) and Rogart (c–e, g) localities. (a, b) Titanites show core–rim zoning from fir-tree bright cores towards dark rims. (c–e) Titanites show different zones with multiple dissolution–reprecipitation features. (f, g) Appinitic titanites from Strontian and Rogart, respectively, show typical sector zoning.

are always present as inclusions in biotite, aligned parallel to the basal cleavage. The chemical zoning pattern within this sample is more complicated than in those from the Strontian granodiorites. Cores usually display fir-tree zoning, surrounded by several successive bright to dark zones (l0–50 μm width; Fig. 2c), which seem to develop following dissolution–reprecipitation episodes (Fig. 2c–e). Such titanites locally contain many Fe–Ti oxide and some apatite inclusions.

Tonalite: samples R2 and RT1
Titanites are large (up to 1.5 mm in length) and euhedral. In RTl, they are often altered and replaced by calcite. Titanite zoning is comparable with that in RHG-l with dissolution–reprecipitation textures observed. The results of several dissolution–reprecipitation events have caused complex zoning made of up to six zones around the core (e.g. Fig. 2e). Although oxides are abundant as inclusions within titanite, apatite inclusions are rarer.

Appinite: samples SR2 and RA1
Titanite is anhedral and larger than that in the granitoids (up to several centimetres; Fig. 2f and g). In SR2 it is interstitial between the main minerals (amphibole, biotite and feldspar), which suggests that it grew late in the crystallization sequence. Titanites from RAl are anhedral–subhedral and in contrast to SR2 do not show any obvious interstitial texture. In both samples, titanite can be texturally in contact with apatite, but rarely contains inclusions. Titanites always have sector and often oscillatory zoning (Fig. 2f and g). However, in contrast to the granitoids, they do not exhibit any systematic core to rim zoning. The sectored and brighter zones can appear either at the edge or in the core. Rarely, a thin and external dark rim is present.

Apatite
Bi–hb granodiorite: samples SR1 and SR3
In both samples, apatite occurs mainly as inclusions within biotite and amphibole and more rarely within feldspar. It is also common as inclusions within titanite and zircon. Apatite grains are either large and subhedral (up to 500 μm in length) or small and euhedral (<300 μm). In CL, they are zoned and comprise an oscillatory zoned core enclosed by an homogeneous rim (<50 μm; Fig. 3a and b). Some crystals are entirely homogeneous in CL.

Granite and tonalites: samples RHG-l, RT1 and R2
Apatites are mainly present within biotite and green amphibole. As for the Strontian granodiorite, apatite inclusions occur within titanite and zircon. CL reveals oscillatory zoning in most of the crystals, which is sometimes absent at the rim (Fig. 3c–e).

Appinite: sample SR2 and RA1
In SR2, two apatite types can be identified: one type is homogeneous in CL and the other has a homogeneous, partly dissolved core and a bright rim (Fig. 3f). These can be linked to different textural locations, the former within feldspar and the latter as inclusions in amphiboles or in late titanite. As feldspar is usually an early crystallizing phase compared with amphibole, it is likely that apatite within feldspar crystallized early and that apatite rims present within titanite crystallized later.

In RAl, apatites are large (up to 1 cm in length; Fig. 3g) and have a significant modal abundance (Table 1). Indeed, the amount of apatite is much higher than that of titanite. This is not the case in SR2, in which the proportion of both phases is roughly the same. Apatite occurs as inclusions within amphibole and feldspar or in contact with titanite. In CL images, apatite textures are similar to the second type of apatite found within SR2, with a dark core showing dissolution features surrounded by a brighter rim (Fig. 3g).

Zircon
Bi–hb granodiorite: samples SR1 and SR3
In these samples, zircons occur within the three main phases (biotite, green amphibole and feldspar) and can be up to 500 μm in length. They are abundant and exhibit typical igneous oscillatory zoning in CL (Fig. 4a and b). Inherited cores are rare.

Granite and tonalites: samples RHG-l, RT1 and R2
Zircons in these samples have the same characteristics as those in the Strontian granodiorite described above. The only difference is that a darker rim (<30 μm) is occasionally observed (Fig. 4e).

Appinites: samples SR2 and RA1
Within SR2 a few zircons have been identified, of which two types could be distinguished. One shows clear igneous oscillatory zoning (Fig. 4f) and the second shows sector zoning. Within RAl zircons were not observed in thin section and only a few tiny crystals could be extracted. Unfortunately, these zircons are extensively cracked and altered (Fig. 4g) and were therefore not suitable for analysis.

RESULTS
LA-ICP-MS *in situ* chemical data for titanite, apatite and zircon in the Strontian and Rogart samples are described below, concentrating on the REE because of their central role in petrogenetic interpretations, with other trace elements discussed as appropriate.
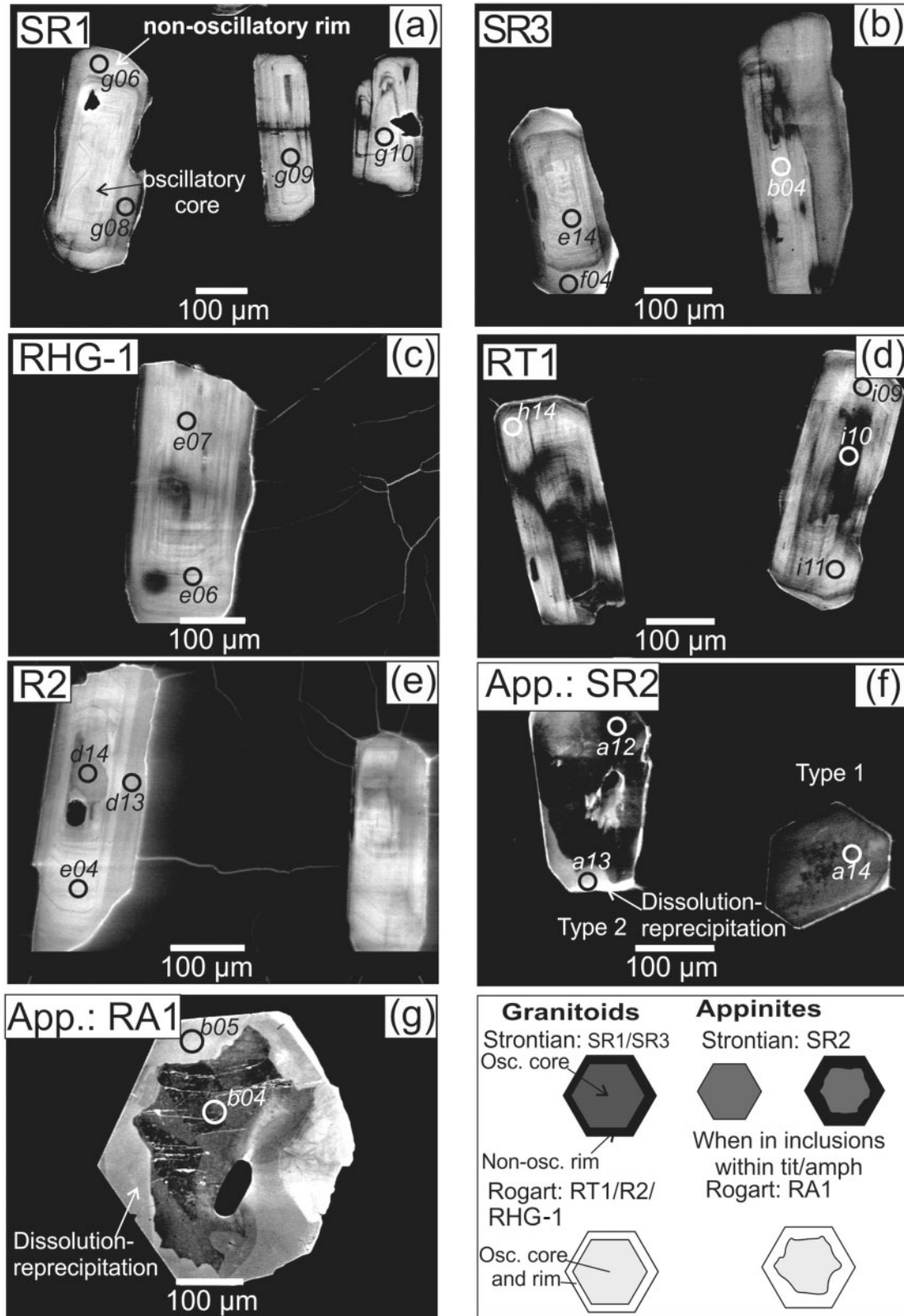
Fig. 3. Cathodoluminescence images of apatite crystals from granitoids (a–e) and appinites (f, g); (a, b, f) Strontian locality and (c–e, g) Rogart locality. (a, b) Apatites from Strontian granitoids comprise oscillatory zoned cores and unzoned rims. (c–e) Apatites from the Rogart granitoids are characterized by oscillatory zoning. (f, g) Apatites from appinitic samples are characterized by a main dark zone (Type 1), which can be dissolved at its rim and reprecipitate a bright rim (Type 2).
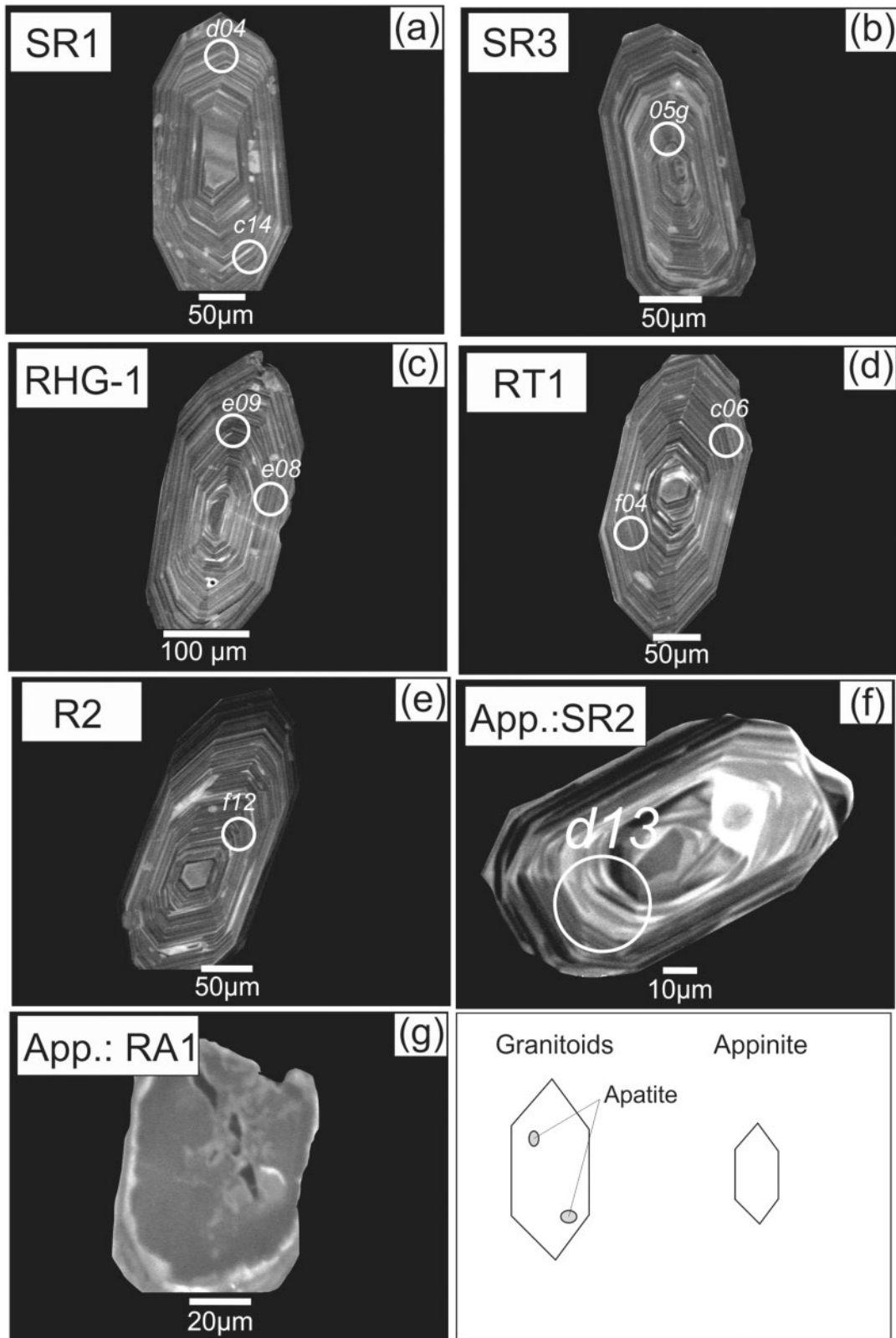
Fig. 4. Cathodoluminescence images of zircons from the Strontian locality [granitoids (a, b); appinite (f)] and the Rogart locality [granitoids (c–e); appinite (g)]. (a–f) Zircons are characterized by typical igneous oscillatory zoning. (g) Typical altered and cracked Rogart appinite zircon.

Titanite chemistry

Rare earth elements

Chondrite-normalized REE patterns are illustrated in Fig. 5. The titanites from the Strontian granodiorite samples are similar but can be divided into three groups (Fig. 5a). The first group (Group 1) has a high REE content and a significant negative Eu anomaly [(Eu/Eu*)$_N$ = 0·56–0·85; Table 2 and Supplementary Data: Electronic Appendix 2] and represent the broad core of the crystals and the fir-tree zones. The second group (Group 2) has lower REE content (especially LREE) and a Eu anomaly which is slightly negative [(Eu/Eu*)$_N$ = 0·75–0·93]. This group of analyses are exclusively from the rims of the crystals. The third group (Group 3) has the lowest REE contents and a positive Eu anomaly [(Eu/Eu*)$_N$ = 1·06–1·59]. This last group is rare and could be characterized only when a darker external rim was present and was wider than the laser spot size (30 μm, Fig. 2a).

Appinitic titanite REE patterns are somewhat different with a general pattern showing a slightly positive Eu anomaly (Fig. 5c), although two groups can be distinguished. Group 1 represents analyses made on bright sector zones. Group 2 represents analyses made on rare external dark rims. Group 1 is LREE enriched with a slightly negative to positive Eu anomaly [(Eu/Eu*)$_N$ = 0·89–1·50]. Different parts of the sector zones have REE patterns that overlap within a limited range of compositions (Fig. 5c); the brightest zones usually have higher REE abundances and the darkest the lowest (Table 2; Supplementary Data: Electronic Appendix 2). The external dark rims have lower LREE contents than Group 1 and are characterized mainly by a negative Eu anomaly [(Eu/Eu*)$_N$ = 0·80–1·51]. Titanites from the Rogart appinite are more enriched in LREE than those in the Strontian appinite and have no Eu anomaly (Fig. 5c). Titanites from this sample are also characterized by a convex-upward shape in the LREE. The different sector zones observed within titanite crystals all have similar concentrations and patterns.

The chondrite-normalized REE patterns of the Rogart granite and tonalites have core patterns (Group 1) with a convex-upward LREE pattern and a negative Eu anomaly similar to that of titanite in the Strontian granodiorite. Rim compositions (Group 2) have lower LREE abundances than Group 1 (Fig. 5b) and have a similar or slightly less pronounced negative Eu anomaly. Rim compositions in the granite sample (RHG-1) vary more than the R2 or RT1 rims, which have a lower LREE content and no Eu anomaly (Table 2; Supplementary Data: Electronic Appendix 2). This could be linked to the two generations of titanite found within the RHG-1 thin section, of which one grew late. Bright dissolution–reprecipitation zones in R2 crystals (Group 3) have a convex-upward LREE pattern and a slightly negative to absent Eu anomaly.

Other trace elements

Previous studies on titanite zoning in the Strontian pluton (Paterson *et al.*, 1989; Paterson & Stephens, 1992) have suggested that the zoned sectors are out of equilibrium with the magma. On the other hand, modelling and recent experimental studies (Watson & Liang, 1995; Hayden *et al.*, 2008) have shown that although the most enriched sector zones do seem to be out of equilibrium (e.g. fir-tree features; FT), other parts of the titanite zones are not and therefore that titanite can be used as a petrogenetic indicator (e.g. Hayden *et al.*, 2008; McLeod *et al.*, 2011). These studies have also shown that the brightest parts of the sector zones preferentially incorporate a substantial amount of certain elements (such as Zr and some REE) on a set of growth surfaces. Such 'enriched' sector zones have been interpreted as representing an area or face of growth entrapment (Watson & Liang, 1995). Watson & Liang (1995) have shown that there is a 'critical ratio of growth rate to lattice diffusivity' above which sector zoning develops, leading to the abnormal enrichment of REE and some trace elements (e.g. Nb and Zr). This was confirmed in a later study (Hayden *et al.*, 2008) in which experiments with titanite crystallization have shown that the Zr content of bright sector zones resulted in an overestimation of the temperature of crystallization of the titanite [see discussion by Hayden *et al.* (2008)]. The FT and bright sector zones in the titanites from our study similarly have a substantially higher Zr content (Table 2; Supplementary Data: Electronic Appendix 2). Although analyses of FT and brightest sector zones always correspond to the highest REE contents (Table 2; Supplementary Data; Electronic Appendix 2), their chondrite-normalized REE patterns are not clearly distinguishable from the other parts of the crystals. Similar to Zr content, FT zone Nb contents are much higher (ranging from 2000 to 3500 ppm) than the non-FT zoned cores of the granodiorite titanites (between 1000 and 1700 ppm). The brightest sector zones of the appinite sample reveal the same systematics, with Nb being much higher than in the other sector zones (Table 2; Supplementary Data: Electronic Appendix 2). Following the results of the experimental and modelling studies (Watson & Liang, 1995; Hayden *et al.*, 2008), these anomalously high Nb and Zr contents in the FT and sector zones are interpreted as being out of equilibrium with the magma composition and will not be considered further here.

Discarding the FT and brightest sector zone data, two trends are apparent within the Strontian granitoid data on a Nb vs Gd plot (Fig. 6a), corresponding to core and rim compositions. Core compositions have a constant Nb content, although Gd generally decreases outwards. Rim analyses correspond to an abrupt decrease in Nb and Gd contents, comparable and parallel to that defined by the appinite titanite compositions.
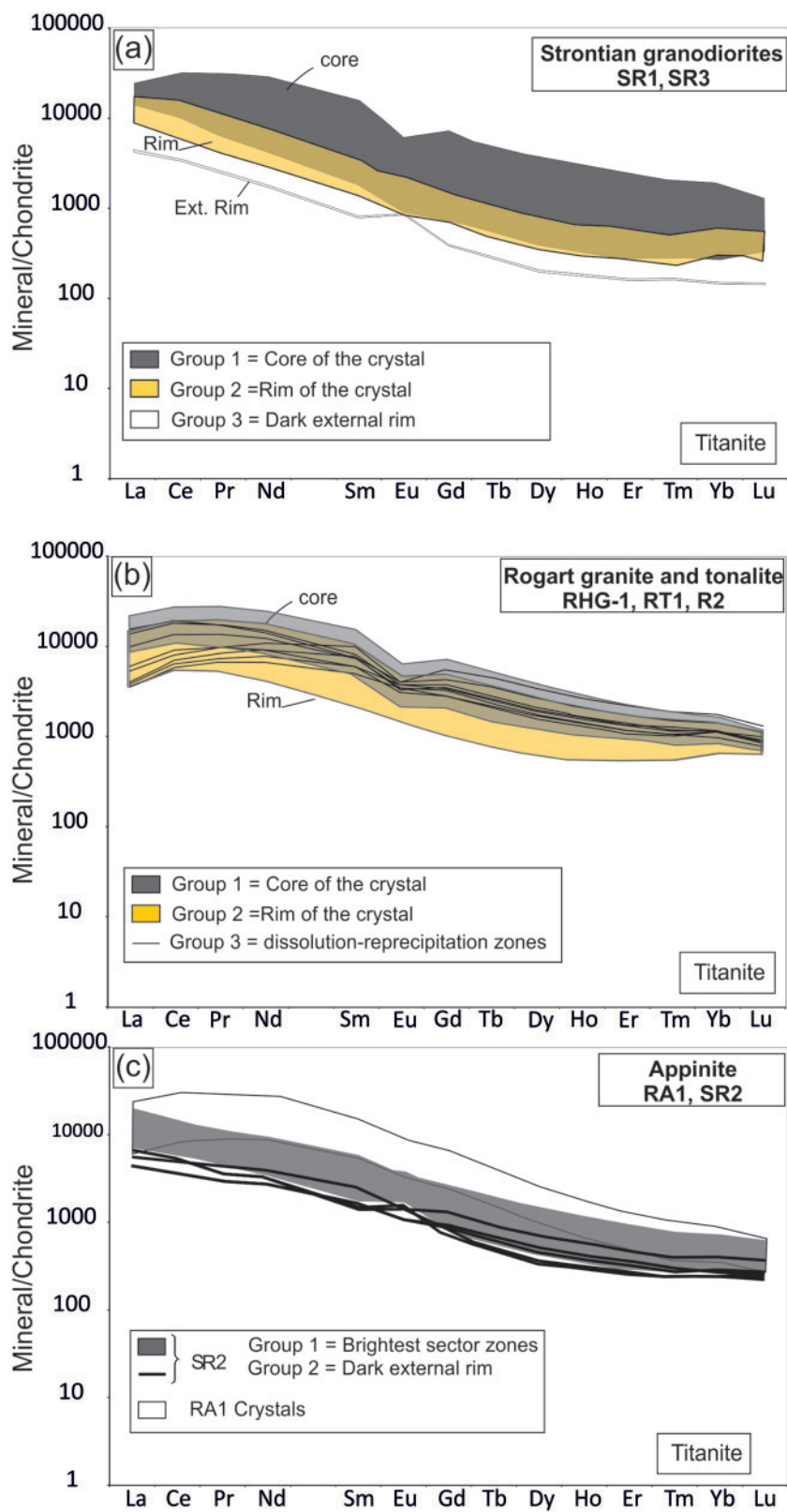
Fig. 5. Chondrite-normalized REE patterns [using McDonough & Sun (1995) chondrite values] for titanites in (a) Strontian granodiorites (SR1, SR3), (b) Rogart granite (RHG-1) and tonalites (RT1, R2) and (c) Rogart and Strontian appinites (RA1, SR2). (See Table 2 and Supplementary Data: Electronic Appendix 2.)

Table 2: Representative analyses of titanite (for full details see Supplementary Data)

Mount	SiO$_2$	CaO	TiO$_2$	V	Cr	Sr	Y	Zr	Nb	La	Ce	Pr	Nd	Sm	Eu	Gd	Tb	Dy	Ho	Er	Tm	Yb	Lu	Ta	(Eu/Eu*)$_N$	(La/Sm)$_N$
RA1 sample—appinite																										
mr07d09	**28·2**	**26·4**	**29·8**	**1140**	**52**	**257**	**2170**	**731**	**1950**	**3990**	**14100**	**2250**	**11100**	**2170**	**467**	**1230**	**135**	**585**	**88**	**188**	**23**	**134**	**15**	**233**	**0·87**	**20·23**
mr30b03*	**29·9**	**26·0**	**32·2**	**1010**	**46**	**263**	**1990**	**1280**	**2110**	**5290**	**17000**	**2470**	**11300**	**2000**	**454**	**1130**	**119**	**511**	**79**	**167**	**21**	**123**	**14**	**101**	**0·92**	**29·22**
mr30c03	**30·8**	**25·7**	**32·0**	**990**	**46**	**256**	**2190**	**1330**	**2240**	**5420**	**17500**	**2520**	**11900**	**2210**	**488**	**1260**	**136**	**570**	**87**	**189**	**23**	**135**	**16**	**150**	**0·89**	**27·27**
mr30a06	32·4	27·2	33·7	1080	51	217	1300	426	652	2240	8090	1320	6390	1250	337	716	78	335	52	108	13	79	10	30	1·09	1·12
mr30a03	32·7	27·8	33·1	1140	86	219	963	362	416	1340	5190	876	4370	898	199	546	59	257	39	87	10	65	7·6	16	0·87	0·93
mr30a05	33·6	27·8	34·2	1200	90	229	1220	415	433	1670	6410	1070	5300	1070	249	646	71	315	48	103	13	78	9·3	16	0·91	0·97
mr30b05*	32·6	26·8	33·0	1210	45	213	1450	528	588	3040	10400	1620	7650	1400	328	813	88	376	57	123	14	86	10	24	0·94	1·36
RT1 sample—granitoid																										
mr07c14	**28·2**	**26·9**	**30·7**	**822**	**172**	**96**	**2540**	**576**	**2500**	**3780**	**12200**	**1760**	**7350**	**1290**	**225**	**784**	**104**	**538**	**99**	**248**	**34**	**220**	**25**	**345**	**0·68**	**1·83**
mr30d13	**32·5**	**26·6**	**33·0**	**809**	**161**	**87**	**2280**	**528**	**1830**	**3200**	**10600**	**1490**	**6250**	**1070**	**191**	**681**	**90**	**466**	**85**	**218**	**30**	**194**	**23**	**168**	**0·68**	**1·87**
ap3a05*	**31·5**	**26·9**	**33·8**	**833**	**191**	**82**	**1720**	**446**	**1460**	**2330**	**7530**	**1030**	**4270**	**726**	**136**	**471**	**61**	**324**	**61**	**164**	**24**	**172**	**21**	**132**	**0·71**	**2·00**
1-mr07d06	30·1	27·6	30·8	877	200	84	1900	485	1400	2470	8210	1200	5080	896	160	525	73	390	72	187	27	187	22	127	0·71	1·72
1-mr30d14	32·1	26·7	32·5	823	197	117	2910	568	1200	3200	11800	1850	8620	1730	277	1080	141	704	121	284	37	214	23	115	0·62	1·16
1-ap3a03*	32·3	27·3	34·2	845	143	86	2360	519	1310	2930	10200	1520	6720	1230	207	777	102	520	93	229	32	194	23	120	0·65	1·49
2-mr07c13	29·2	28·8	32·4	790	223	102	1350	322	1050	1170	4040	620	2720	518	141	350	48	253	48	128	19	140	18	50	1·01	1·41
2-mr30d06	34·1	27·8	34·0	778	204	108	1860	372	1310	1610	5650	854	3850	737	180	510	68	365	69	175	26	183	24	75	0·89	1·36
2-ap3a06*	31·3	27·5	33·7	735	206	99	1580	362	1190	1640	5760	836	3740	713	166	472	62	323	60	154	22	148	18	75	0·87	1·44
RHG-1 sample—granitoid																										
1-mr08a04*	28·0	26·7	29·4	811	191	78	1850	481	1220	2940	9330	1290	5300	883	164	549	72	381	69	171	24	160	20	93	0·72	2·08
1-mr08a05	27·7	27·3	30·6	751	159	89	2300	511	1080	3440	11500	1680	7380	1330	222	835	108	546	93	222	30	174	20	86	0·64	1·62
2-mr08a03*	28·5	28·3	30·8	882	224	71	924	308	1240	1250	3800	487	1910	301	80	202	28	149	29	88	14	107	16	64	0·99	2·59
2-mr08a07	27·9	27·3	30·0	783	186	82	2080	491	1160	3160	10400	1480	6320	1100	190	675	90	465	81	197	27	174	20	87	0·67	1·79
Rp-mr08a06	29·7	27·2	30·8	737	124	86	2040	539	1470	3710	11800	1630	6720	1080	192	662	85	431	77	190	26	169	20	127	0·69	2·15
R2 sample—granitoid																										
mr08a12*	**27·9**	**26·0**	**30·0**	**841**	**146**	**89**	**3570**	**644**	**2220**	**3920**	**14600**	**2350**	**11100**	**2220**	**341**	**1340**	**180**	**906**	**152**	**350**	**44**	**260**	**27**	**282**	**0·60**	**1·10**
mr08a13	**28·3**	**26·9**	**29·8**	**813**	**183**	**85**	**2450**	**592**	**1860**	**3050**	**10600**	**1570**	**6810**	**1240**	**208**	**760**	**103**	**537**	**97**	**243**	**32**	**207**	**24**	**241**	**0·65**	**1·54**
1-mr08a11*	28·8	27·4	30·6	900	215	82	2290	507	1340	2520	9000	1380	5970	1110	187	692	93	485	87	221	30	202	24	121	0·65	1·42
1-mr08a14*	28·8	27·4	30·1	855	231	88	2120	483	1300	2560	8560	1250	5350	948	173	582	80	437	80	207	29	198	25	108	0·71	1·69
2-mr08a10*	28·9	28·1	31·2	821	193	65	1850	360	1400	1620	5710	862	3770	748	158	500	69	368	66	176	26	176	23	97	0·79	1·35
2-no10d14	32·8	27·9	35·5	704	219	89	1470	307	1250	1010	3830	611	2920	586	152	400	55	299	54	147	21	145	20	53	0·96	1·08
Rp-mr08a08	27·7	28·2	30·8	716	119	57·5	2050	349	1580	1440	5610	904	4250	899	177	604	81	417	77	191	28	172	21	120	0·73	1·00
Rp-mr08a09	27·8	27·9	30·9	699	104	60·1	2050	335	1690	1430	5640	917	4250	893	176	603	82	434	77	194	27	182	21	131	0·73	1·00

(continued)

Table 2: Continued

Mount	SiO$_2$	CaO	TiO$_2$	V	Cr	Sr	Y	Zr	Nb	La	Ce	Pr	Nd	Sm	Eu	Gd	Tb	Dy	Ho	Er	Tm	Yb	Lu	Ta	(Eu/Eu*)$_N$	(La/Sm)$_N$
SR2 sample—appinite																										
no09d11	**34.7**	**28.3**	**34.9**	**789**	**250**	**168**	**951**	**1080**	**1480**	**4390**	**8380**	**932**	**3500**	**548**	**201**	**331**	**43**	**212**	**39**	**96**	**14**	**93**	**12**	**47**	**1.44**	**5.00**
no10a08*	**34.0**	**28.6**	**36.9**	**820**	**269**	**164**	**1090**	**895**	**1250**	**3870**	**7660**	**892**	**3530**	**565**	**199**	**359**	**45**	**233**	**44**	**105**	**14**	**104**	**13**	**37**	**1.35**	**4.28**
no10a10*	35.1	29.4	36.6	857	409	114	697	352	201	1880	3970	466	1920	326	108	210	28	144	27	70	10	65	8.7	6.5	1.26	3.60
no10a12	34.2	28.9	35.2	842	450	120	487	376	233	1860	3680	407	1580	258	95	155	20	104	18	46	6.7	46	6.5	8.4	1.45	4.50
2-no10a11*	34.8	29.1	35.9	855	481	127	451	337	223	1720	3370	369	1440	227	88.8	141	18	92.9	17	45	6.6	42	5.9	4.7	1.51	4.73
2-no10b06	34.1	29.2	36.4	919	522	95.7	821	431	272	1390	3130	418	1900	374	82.4	264	35	181	32	79	11	68	10	10	0.80	2.32
SR1 sample—granitoid																										
no08c06*	**34.6**	**27.8**	**36.5**	**859**	**96**	**72**	**2130**	**669**	**2240**	**4880**	**14800**	**1910**	**7490**	**1160**	**198**	**694**	**88**	**452**	**82**	**205**	**29**	**185**	**21**	**351**	**0.67**	**2.63**
no08d03	**33.0**	**27.8**	**34.5**	**940**	**136**	**69**	**3310**	**770**	**2060**	**4630**	**15600**	**2370**	**10700**	**1990**	**302**	**1260**	**161**	**806**	**135**	**318**	**40**	**239**	**27**	**396**	**0.58**	**1.45**
1-no08c13	33.5	28.1	35.0	851	175	65	1310	601	1030	3900	10700	1280	4680	660	120	392	49	256	47	126	19	128	17	113	0.72	3.69
1-no08c14*	33.9	28.1	34.9	887	167	68	2090	659	1620	4040	12700	1720	7030	1180	195	708	90	454	80	200	28	172	21	264	0.65	2.14
2-no08c09	32.8	28.1	35.4	774	114	64	622	471	797	2790	5410	531	1900	294	71	194	26	131	23	58	8.2	53	7.8	27	0.91	5.93
2-no08c12*	33.0	28.1	34.7	741	134	65	524	520	721	2630	5080	481	1620	235	56	146	20	102	19	50	6.9	54	8.5	36	0.92	6.99
2-no08d14	32.7	28.8	35.1	783	131	65	698	471	674	2740	5340	536	1930	314	79	214	28	150	27	72	10	73	10	30	0.93	5.45
3-no08c10	32.6	28.8	35.2	860	125	61	652	333	589	2370	4730	515	1970	332	93	217	27	146	26	62	8.5	55	7.2	20	1.06	4.46
3-no08c11*	34.0	28.8	35.4	964	125	50	273	212	265	1070	2170	220	806	117	51	80.1	10	50	9.8	26	4.1	24	3.7	1.8	1.59	5.71
SR3 sample—granitoid																										
ap3e04*	**31.9**	**25.7**	**33.0**	**852**	**230**	**64.0**	**3290**	**635**	**2140**	**4770**	**16200**	**2360**	**10900**	**2060**	**310**	**1280**	**166**	**830**	**138**	**317**	**40**	**233**	**26**	**364**	**0.58**	**1.45**
mr07a05	**28.7**	**27.8**	**31.4**	**741**	**109**	**72.8**	**826**	**759**	**2110**	**4850**	**10900**	**1080**	**3420**	**411**	**82**	**234**	**29**	**147**	**29**	**76**	**12**	**86**	**13**	**260**	**0.81**	**7.37**
1-ap3e05*	32.7	26.8	33.4	835	147	62.6	1730	612	1080	3640	10700	1390	5510	854	150	542	67	349	63	162	23	155	20	134	0.67	2.66
1-no09b13	32.1	27.8	34.5	716	134	67.4	1520	512	1190	3820	8460	987	3820	615	141	420	56	299	57	143	20	133	18	116	0.85	3.88
2-mr07a03*	29.5	28.5	31.8	764	141	64.7	526	481	836	2640	5240	513	1690	231	55	149	19	101	19	49	7.3	55	8.2	47	0.90	7.14
2-ap3e03	32.4	27.9	33.9	716	119	62.8	630	470	869	2920	5560	530	1880	282	66	199	25	129	24	61	8.4	61	9.0	34	0.85	6.47
2-no09a03	34.2	28.6	37.6	787	181	58.7	844	570	1260	3210	7270	742	2490	325	63	202	27	137	27	79	12	91	14	116	0.75	6.17

1, core compositions; 2, rim compositions; 3, dark external rim; Rp, reprecipitation feature. Analyses in bold are from fir-tree (FT) and extremely bright sector zones. SiO$_2$, CaO and TiO$_2$ are reported in wt %, the other elements in ppm.
*Analyses plotted in Fig. 2.
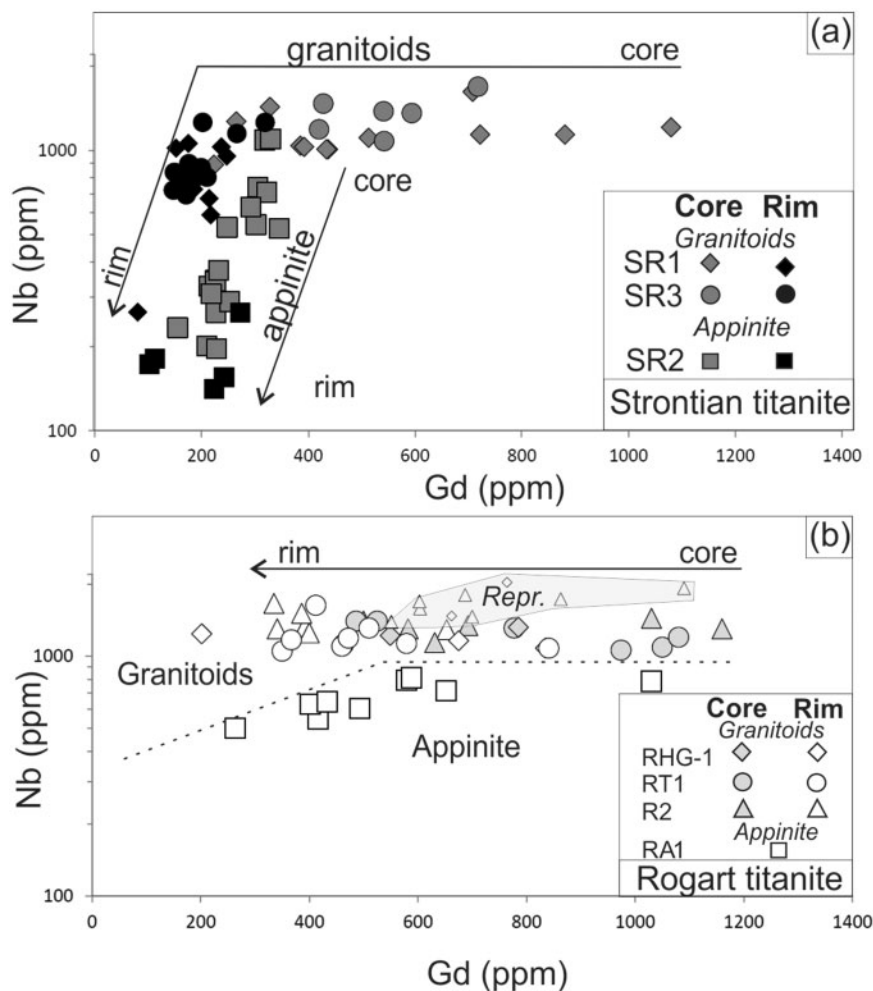
Fig. 6. Nb (ppm) versus Gd (ppm) for titanite from (a) Strontian and Rogart (b) localities. Data reported in this figure do not include analyses of the FT or bright sector zones (See Table 2; Supplementary Data: Electronic Appendix 2). Reprecipitation zones are indicated by smaller symbols and the shaded field.

On a $(Eu/Eu^*)_N$ versus $(La/Sm)_N$ diagram (Fig. 7a), two trends (cores and rims) can again be identified within the granitoid samples. Core compositions mostly plot between unity and ~5 $[(La/Sm)_N]$ with some core analyses and all the rims plotting above five; $(La/Sm)_N$ increases and the negative Eu anomaly reduces towards the rim. One analysis representing the dark external rim and two analyses of the rim within SR1 have positive Eu anomalies and plot in the same area as the appinite trend. The $(La/Sm)_N$ ratio within Strontian appinite shows a positive correlation with $(Eu/Eu^*)_N$.

Hayden *et al.* (2008) have shown that the Zr content of titanite is temperature dependent. Considering that the different plutons cooled at similar pressures during titanite crystallization [13–14 km depth, following Tyler & Ashworth (1983)], Fig. 7b can be interpreted in terms of temperature (proxied by Zr) versus HREE content (Y being a proxy for the HREE). Once again, two groups

can be distinguished following core–rim compositions. Core compositions vary from high Y contents (>3000 ppm) towards lower Y contents (~1000 ppm, external part of the core) at comparable Zr contents (500–700 ppm). Rim compositions of Y plot below 1000 ppm but show more rapidly decreasing Zr contents (ranging from 600 to ~400 ppm). Rims from SR1 have much lower Zr contents (~200 ppm). Titanites from the Strontian appinite show a similar range of Y concentrations (from ~1000 to ~500 ppm; Fig. 7b) to titanite rims from the granitoids. The Zr content of titanite from the appinite decreases from ~650 ppm to 100 ppm in the dark external rims. Thus, applying the Zr-in-titanite thermometer [Hayden *et al.* (2008), who estimated the uncertainty at ±20°C], titanite in the Strontian granitoids began to crystallize at ~772°C and finished at ~709°C, based on maximum Zr contents in the cores towards minimum Zr contents in the rims (Table 2; Supplementary Data: Electronic
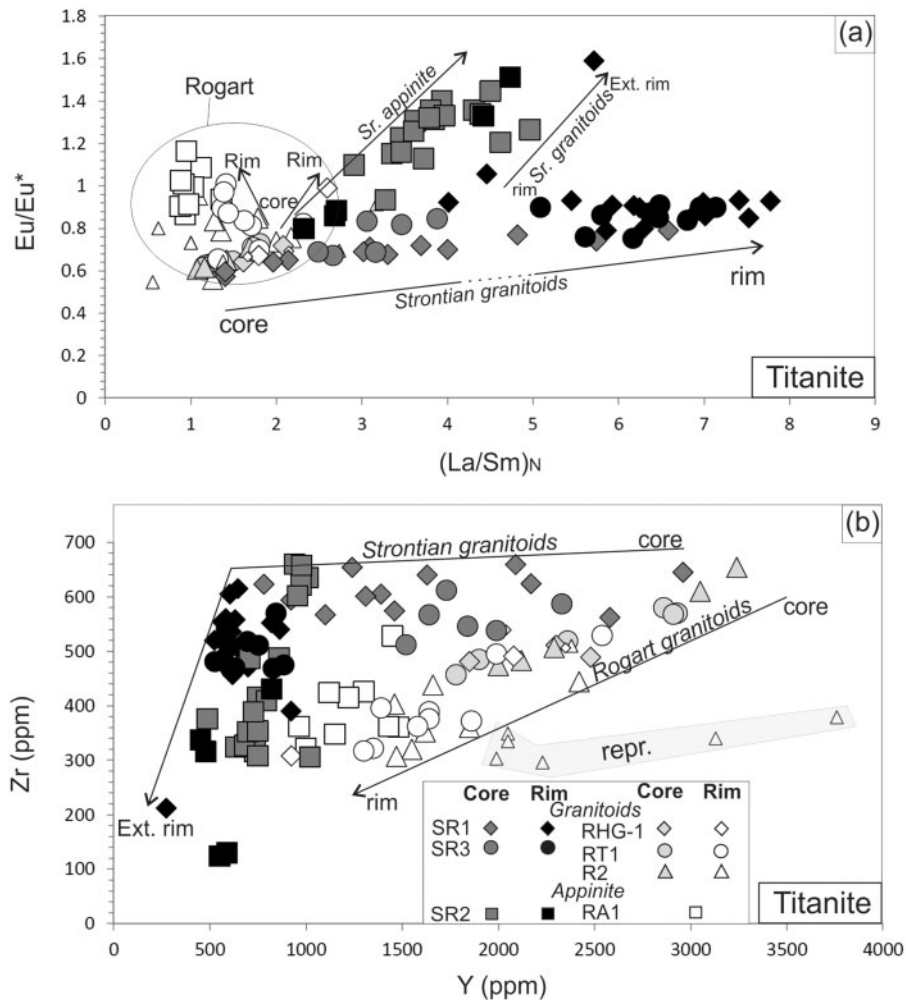
Fig. 7. (a) Eu/Eu* versus (La/Sm)$_N$ for the Strontian and Rogart granitoid titanite compositions and the appinite titanite compositions. Core and rim compositions are differentiated. (b) Zr content (ppm) versus Y content (ppm) for Rogart and Strontian titanites. Reprecipitation analyses are indicated by smaller symbols and the shaded field.

Appendix 2). Using maximum and minimum values within the Strontian appinite, titanites crystallized between ∼772°C and ∼682°C. These values are maximum estimates, assuming the activities of TiO_2 and SiO_2 in our calculations were unity as quartz is present and the amount of titanite in the samples is more likely to reflect a high $aTiO_2$. Using a lower activity of $aTiO_2 = 0.5$ [suggested as the lower limit for typical crustal rocks by, for example, Ferry & Watson (2007) and Hayden & Watson (2007)] in the calculations would decrease the temperature results by about 50°C.

As for the titanites from Strontian, those from Rogart (Table 2; Supplementary Data: Electronic Appendix 2) also show a wide compositional scatter between FT and sector zones, consistent with disequilibrium conditions. Removing these FT and bright sector zones, the data show a single Nb vs Gd trend within the granitoid samples

(Fig. 6b). Although Gd content decreases from the cores towards the rims (from ∼1100 ppm to 200 ppm), Nb contents are mostly between 1000 and 1400 ppm with analyses from areas interpreted as having undergone reprecipitation being higher (up to 2030 ppm). Except for one analysis plotting at extremely high Nb and Gd contents, the appinitic titanites define a positive correlation between Gd and Nb.

Rogart granite and tonalite analyses are also plotted on the (Eu/Eu*)$_N$ versus (La/Sm)$_N$ diagram (Fig. 7a). Core values plot within the core trend of Strontian analyses. However, the rim compositions are different with (La/Sm)$_N$ values in the range 1–3 and a Eu anomaly tending towards unity. The spread of titanite compositions in Rogart is more restricted than in Strontian (Fig. 7a). Similarly, the appinite values plot in a narrow range of 1–2 in (La/Sm)$_N$ ratio and around unity for (Eu/Eu*)$_N$.

Although $(Eu/Eu^*)_N$ values are comparable with those for the Strontian appinite, the $(La/Sm)_N$ ratio is much lower in Rogart.

Zr and Y data are plotted in Fig. 7b. In contrast to the Strontian granitoid titanites, those in Rogart define a single trend with Zr and Y contents decreasing from cores ($Y = 3240$ ppm) toward rims ($Y = 924$ ppm). Zr content varies from $\sim$654 ppm in the cores towards 303 ppm within the rims corresponding to temperatures between $\sim$771°C and $\sim$728°C. The titanites from the appinites crystallized between $\sim$759°C and $\sim$731°C.

Apatite chemistry

Chondrite-normalized REE patterns for apatites from the Strontian granodiorite samples (Samples SR1 and SR3) are subparallel and define two groups (Fig. 8a). One group (Group 1) has higher REE contents and a negative Eu anomaly $[(Eu/Eu^*)_N = 0{\cdot}47{-}0{\cdot}93]$, whereas the second group has lower REE contents and a weaker negative Eu anomaly $[(Eu/Eu^*)_N = 0{\cdot}78{-}0{\cdot}94]$. These two groups correspond, respectively, to analyses made in the oscillatory zoned cores and the rims of the apatite crystals (Fig. 3a and b). Both groups have enriched LREE relative to middle REE (MREE). The $(La/Sm)_N$ ratio, representing the slope of the LREE, is plotted versus Gd, representing the MREE concentrations, to illustrate the characteristics of the two apatite groups (Fig. 9). Figure 9a shows that two apatite compositions, reflecting core and rim compositions, can be distinguished within the granodiorite. As for titanite (Fig. 5a), apatite records a distinct change in REE content during its growth. A Ce versus Y diagram also highlights a compositional gap in apatite between cores and rims (Fig. 9c). Minimum Ce concentrations in the cores are $\sim$2300 ppm and maximum Ce values for rim compositions are $\sim$1500 ppm. Interestingly, no other trace elements apart from the REE show systematic variations between core and rim compositions.

The appinite sample (SR2) has apatite REE patterns evolving continuously from high and flat LREE–MREE content with a strong negative Eu anomaly towards higher LREE/MREE and slightly negative to absent Eu anomaly (Fig. 8c). The lower REE contents correspond to apatite rims when they occur as inclusions in amphibole and titanite or simply in contact with them. Apatites in appinites display a general increase in $(La/Sm)_N$ and decrease in Gd content toward the bright rims of the crystals (when this rim has been identified—see petrography description; Figs 3f, h and 9a). Figure 9a highlights the decrease of MREE (Gd) in apatite rims in contact with late phases such as titanite.

Chondrite-normalized REE patterns for apatite from the Rogart granite and the two tonalites are illustrated in Fig. 8b. In contrast to the Strontian apatites, the REE patterns of cores and rims overlap; consequently the core and rim patterns of the various samples have been merged for easier inter-sample comparison. The R2 REE patterns are tightly clustered with a flat LREE pattern and a slight negative Eu anomaly. RT1 is similar, but also has more enriched LREE compared with MREE. The RHG-1 patterns are more clustered and in general have the lowest normalized abundances of the three samples. However, the RHG-1 patterns show exactly the same characteristics (flat LREE pattern and slight negative Eu anomaly) as the other two samples. Core compositions of the RHG-1 apatite tend to have the highest total REE (Table 3; Supplementary Data: Electronic Appendix 3). For all three samples, despite overlap, there is a trend to lower total REE concentration from cores towards rims (Table 3; Supplementary Data: Electronic Appendix 3). Apatite compositions in the Rogart tonalites or granite do not show abrupt changes in composition. They are characterized by large variations in Gd and small variations in $(La/Sm)_N$ (Fig. 9b).

Apatite chondrite-normalized REE patterns for the Rogart appinite are different from the Strontian appinite, with a flat LREE pattern and a slightly negative to absent Eu anomaly (Fig. 8c). Analyses either from cores or rims are tightly clustered and do not show significant differences. The flat LREE and the Eu anomaly of apatite REE patterns in the Rogart appinite have similar characteristics to the titanite from the same location (Fig. 5c).

Apatite $(La/Sm)_N$ values are around two, as for the other more evolved samples (Fig. 9b). Appinite apatites have Gd contents ranging from $\sim$200 ppm to $\sim$80 ppm. Appinite and tonalites or granite cannot be distinguished based on their apatite composition in this diagram and have a rather constant $(La/Sm)_N$ ratio. There is a positive correlation between Ce and Y within each Rogart sample, with a general continuous decrease of these elements from cores toward rims (Fig. 9c).

Zircon

Chondrite-normalized REE patterns for zircon within the Strontian granodiorite (SR1 and SR3) are homogeneous and have typical igneous zircon REE patterns (e.g. Hoskin & Schaltegger, 2003) with large positive Ce anomalies, negative Eu anomalies and strong HREE enrichment (Fig. 10a). No systematic core to rim variations have been observed, in contrast to apatite and titanite (Figs 5a and 8a). Appinitic zircons have similar REE patterns, although the REE content is systematically higher. This is opposite to the Belousova $et\ al.$ (2002b) compilation of zircon data, which infers an increase of REE content within zircon from ultramafic toward granitoid compositions. Generally the Th/U ratio is <0·5 for igneous zircons (Hoskin & Schaltegger, 2003) and although the Th/U values in zircons from our granitoids are consistent with this, the appinitic sample has slightly higher Th/U (Th/U $\sim$0·5–1·6, Table 4; Supplementary Data: Electronic Appendix 4).
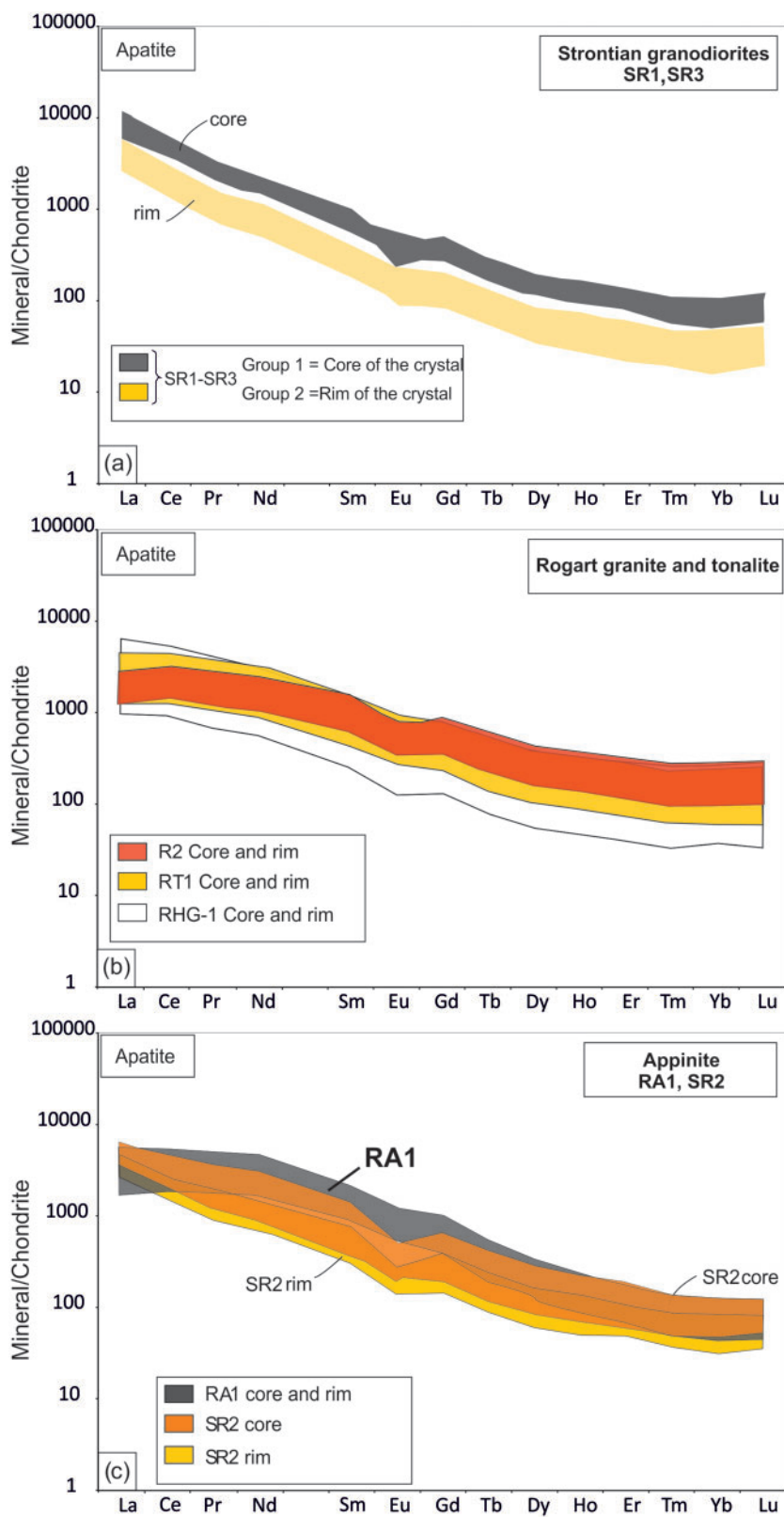
Fig. 8. Chondrite-normalized REE patterns for apatites in (a) Strontian granodiorites (SR1, SR3), (b) Rogart granite (RHG-1) and tonalites (RT1, R2) and (c) Rogart and Strontian appinites (RA1, SR2). (See Table 3 and Supplementary Data: Electronic Appendix 3.)
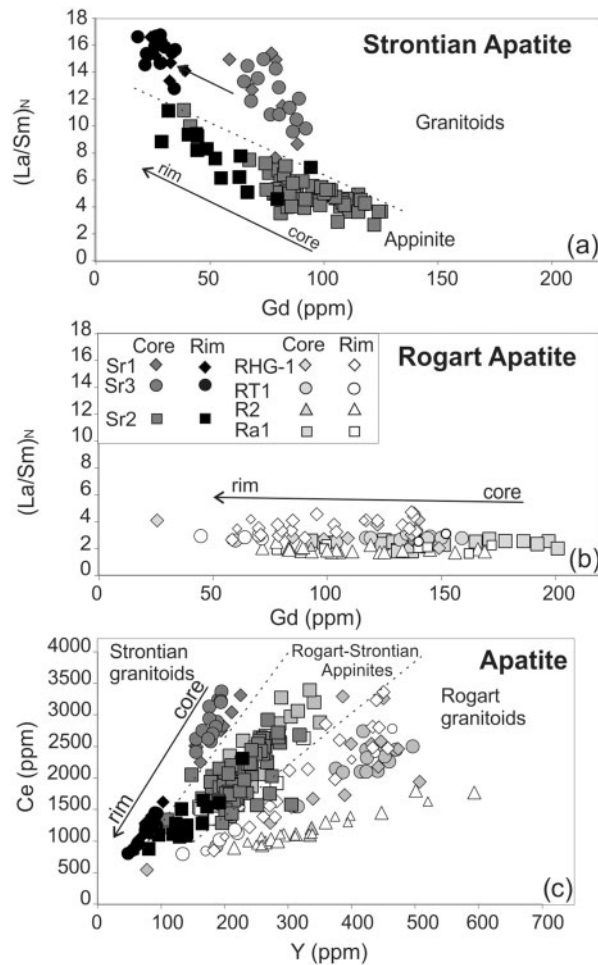
Fig. 9. (a, b) $(La/Sm)_N$ versus Gd (ppm) for apatites from (a) Strontian and (b) Rogart localities. (c) Ce (ppm) versus Y (ppm) for apatites from the Strontian and Rogart localities. Analyses of cores and rims in the granitoids and appinitic samples are distinguished in these figures. In (a) and (c), dotted lines separate granitoids and appinite analyses.

The Rogart tonalites or granite zircons have comparable REE patterns and concentrations to those from Strontian (Fig. 10b). Other trace elements analysed within these zircons do not show any variation between core and rim zones (Table 4; Supplementary Data: Electronic Appendix 4).

DISCUSSION

Petrogenetic records during apatite and titanite crystallization

Accessory mineral composition data from the Rogart and Strontian plutons provide constraints on their crystallization history, particularly in terms of *in situ* crystal fractionation and mixing processes during the crystallization of the magmas.

Saturation of accessory phases

Zircon saturation temperature estimates for granitoids have been made for several decades (e.g. Larsen, 1973; Watson, 1979; Watson & Harrison, 1983; Barrie, 1995, and reference therein; Miller *et al.*, 2003; Harrison *et al.*, 2007; Fu *et al.*, 2008) and have promoted significant understanding of zircon crystallization behaviour in plutons. However, similar data have not been intensively obtained for apatite and titanite since the work of Harrison & Watson (1984) and Green & Pearson (1986). Hoskin *et al.* (2000), in a detailed study of a cogenetic suite of plutonic rocks (Boggy Plain pluton, Australia), described the variation of titanite, apatite and zircon trace element chemistry and used an integrated approach to identify accessory mineral saturation during differentiation. Despite the value of such work, there is a lack of data for other pluton chemistries and geological settings. Several studies [including that by Hoskin *et al.* (2000)] have shown that zircon usually saturates in felsic melts ($SiO_2 \geq 65\%$) but not in those that are less evolved. In the Boggy Plain suite, Hoskin *et al.* (2000) estimated that apatite probably saturates throughout the range of compositions (aplite to diorite) whereas titanite was interpreted as never saturating within the suite. Titanites in these samples were anhedral (except for the most evolved samples) and their abundance was limited.

In contrast to Boggy Plain, all the granitoids from our study are extremely rich in accessory phases (titanite, apatite, zircon; >3% modal proportion). These are euhedral and present as inclusions within all of the rock-forming minerals, strongly suggesting that saturation has been reached. Zircons are large, abundant and contain apatite inclusions. Apatites are large, euhedral in every sample and have been found as inclusions in the other accessory phases (titanite and zircon). These textural relationships suggest that the three accessory minerals grew simultaneously, although apatite might have started to crystallize slightly earlier. The homogeneous composition of apatite cores in these samples does not, however, necessarily support this last statement. In the appinites, apatite is commonly found as inclusions within all the rock-forming minerals and occasionally within titanite, but is not found within zircon. Therefore, either apatite could have saturated and stopped crystallizing before zircon crystallization or the low abundance of zircon may obscure the relationship between these minerals. In appinite SR2, titanite is abundant, anhedral and interstitial, and is therefore interpreted to have crystallized late, possibly in residual melt pools, as described by Hoskin *et al.* (2000). In contrast, titanite in RA1 is anhedral–subhedral, but not interstitial, and therefore might have saturated and started to crystallize slightly earlier. Zircons are tiny, extremely rare and free of apatite inclusions, and are therefore interpreted as not crystallizing early in these ultramafic

Table 3: Representative analyses of apatite (for full dataset see Supplementary Data)

Analysis Nb	P_2O_5	CaO	V	Sr	Y	Zr	La	Ce	Pr	Nd	Sm	Eu	Gd	Tb	Dy	Ho	Er	Tm	Yb	Lu	Pb	Th	U	$(Eu/Eu^*)_N$	$(La/Sm)_N$
RA1 sample—appinite																									
1-ap04b04*	44·30	55·4	31·80	2550	236	1·6	645	1910	274	1310	221	48	137	12	56	8·6	18	2·2	14	1·8	14	36	22	0·84	1·82
1-ap04b06	42·50	54·7	39·20	2650	229	4·8	1000	2590	331	1520	244	53	142	14	55	8·8	20	2·4	13	2·2	15	37	13	0·87	2·56
1-ap04b07	41·00	53·1	35·80	2370	208	3·1	871	2350	291	1310	206	46	125	12	51	7·3	16	1·8	12	1·8	13	41	19	0·87	2·64
R-ap04b05*	44·20	55·0	7·46	2610	140	<0·26	397	1140	162	762	128	30	78	7	29	5·1	11	1·3	7	1·1	12	25	26	0·90	1·94
R-ap04d06	44·00	55·4	9·04	2730	163	0·6	565	1510	198	952	152	33	100	9	40	5·7	14	1·3	9	1·3	13	25	24	0·81	2·32
R-sp04f14	42·00	55·0	39·90	2380	324	4·0	1030	2630	373	1700	283	55	172	17	71	11·5	25	3·0	18	2·4	13	42	17	0·76	2·27
R2 sample—granitoid																									
1-ap04d14*	40·60	55·1	10·40	786	334	2·1	363	1100	147	681	139	26	106	13	63	11·8	31	3·9	25	4·1	9	55	49	0·65	1·63
1-sp03c09	44·10	55·2	8·46	872	337	0·5	449	1210	163	699	129	24	93	12	57	11·3	28	3·8	23	3·8	8	33	12	0·68	2·17
2-ap04c04	46·00	55·2	7·02	862	215	0·4	309	898	113	499	93·4	20	72	8	39	7·7	19	2·4	15	2·6	7	29	18	0·73	2·07
2-ap04e04*	45·30	55·2	5·98	897	312	0·3	382	1110	150	684	136	26	102	12	58	10·8	27	3·7	21	3·5	8	37	18	0·67	1·75
2-sp03b10	42·70	55·2	9·54	870	447	0·5	554	1450	199	901	179	33	145	18	88	17·0	40	4·9	34	5·3	9	53	16	0·62	1·93
2-sp03d05	42·40	55·2	6·71	847	273	0·4	380	1030	134	612	115	23	90	11	52	10·2	26	3·1	22	3·7	8	33	15	0·68	2·06
3-ap04d13*	47·40	55·3	6·58	895	284	0·3	339	1000	131	611	117	24	93	11	55	10·5	26	3·2	21	3·5	9	31	16	0·69	1·81
RT1 sample—granitoid																									
1-ap04h13	40·00	55·3	8·63	982	315	1·0	558	1550	197	844	138	33	104	12	59	11·0	28	3·4	23	3·7	7	55	48	0·83	2·53
1-ap04i10*	41·40	55·3	16·80	1060	187	0·9	355	920	120	514	84·3	21	60	7	34	6·8	17	2·0	15	2·4	7	43	33	0·89	2·63
1-sp04c05	44·50	55·0	9·27	1020	441	1·4	801	2110	279	1220	193	48	139	16	78	15·6	39	5·3	33	5·3	7	69	34	0·89	2·59
RT1 sample—granitoid																									
2-ap04h14*	42·30	54·7	9·08	1050	450	1·8	926	2460	297	1290	198	53	145	16	78	15·8	40	5·1	33	6·0	9	74	31	0·96	2·92
2-ap04i09*	41·30	55·1	8·68	1070	470	2·0	935	2450	306	1300	207	52	150	17	82	16·4	43	5·6	34	6·0	9	79	38	0·90	2·82
2-ap04i11*	40·60	55·0	8·75	1020	452	2·1	871	2340	289	1230	195	51	144	16	82	16·1	40	5·7	36	5·8	8	81	35	0·92	2·79
2-sp04b05	45·50	55·0	8·44	1010	375	1·2	786	2150	273	1120	174	39	117	13	66	12·6	33	4·4	30	4·9	7	60	27	0·83	2·82
3-sp04b06	43·40	55·0	5·43	1060	134	0·2	286	798	94·9	400	60·4	15	45	5	26	4·8	12	1·4	10	1·5	5	18	15	0·90	2·96
3-sp04c06	43·00	55·0	7·05	1020	220	0·9	443	1130	145	633	99·6	24	71	8	41	7·9	20	2·6	16	2·9	6	38	32	0·88	2·78
3-sp04c08	45·50	55·0	7·13	1060	192	0·3	397	1020	131	554	86·6	22	64	7	35	6·4	17	2·1	14	2·3	6	26	26	0·91	2·86
RHG-1 sample—granitoid																									
1-sp03d10	42·40	55·0	8·23	870	272	0·3	523	1290	160	701	114	23	85	9	46	8·9	23	3·2	22	3·3	8	25	13	0·73	2·86
1-sp03e07*	41·90	55·0	10·70	862	446	1·5	1050	2580	320	1290	201	40	139	16	76	15·3	40	5·2	35	5·7	8	82	42	0·73	3·26
1-sp03f05	43·30	55·0	8·35	867	339	1·1	616	1670	214	900	141	28	99	12	56	11·0	29	4·1	27	4·1	8	46	19	0·72	2·73
1-sp03f10	42·00	55·0	9·93	974	450	1·3	1470	3260	370	1410	198	39	138	16	77	15·1	38	5·2	36	5·4	10	74	24	0·72	4·64
2-ap04f06	42·60	55·2	9·37	896	433	1·2	1030	2810	320	1280	188	37	139	15	76	14·1	37	4·9	36	5·8	11	70	21	0·70	3·42
2-ap04f07	43·50	55·0	8·27	926	305	0·6	588	1540	195	818	130	27	90	11	49	9·3	25	3·3	20	3·5	8	46	16	0·77	2·82
2-sp03e06*	44·30	55·0	8·50	900	282	0·5	660	1630	195	799	122	26	84	10	47	9·6	24	3·4	21	3·6	8	48	16	0·77	3·38
2-sp03e08	42·60	55·0	9·00	894	457	1·3	1050	2470	308	1210	187	39	136	16	76	15·4	37	5·5	37	6·1	9	64	19	0·75	3·51
3-ap04i10	42·60	55·2	7·09	858	205	0·2	537	1390	165	592	94·6	19	70	8	37	7·3	18	2·4	16	2·4	9	32	21	0·70	3·54
3-sp03e10	42·80	55·0	7·59	868	183	0·2	329	852	107	460	76·7	16	58	7	30	5·8	15	2·0	14	2·1	6	27	21	0·74	2·68
3-sp03f08	42·40	55·0	8·24	972	439	1·2	1490	3230	365	1410	197	39	137	16	77	14·6	38	5·1	35	5·2	10	73	22	0·72	4·72

(continued)

Table 3: Continued

Analysis Nb	P_2O_5	CaO	V	Sr	Y	Zr	La	Ce	Pr	Nd	Sm	Eu	Gd	Tb	Dy	Ho	Er	Tm	Yb	Lu	Pb	Th	U	$(Eu/Eu^*)_N$	$(La/Sm)_N$
SR1 sample—granodiorite																									
1-ap04f13	42·40	55·4	10·80	572	225	1·8	2680	3310	263	869	112	29	79	8	42	8·3	21	2·4	16	2·7	11	136	47	0·93	14·94
1-ap04f14	43·80	55·4	12·40	571	211	1·7	2540	3040	249	822	103	27	77	8	38	7·4	18	2·4	17	2·8	11	125	40	0·92	15·40
1-ap04g05	41·50	55·0	8·90	697	154	1·1	2030	2510	201	664	84·8	19	59	6	29	5·5	14	1·7	12	1·8	9	62	17	0·81	14·95
1-ap04g09*	43·90	55·0	16·30	623	162	0·7	1440	2250	219	809	118	13	79	8	39	5·9	14	1·6	8	1·6	9	72	25	0·41	7·62
1-ap04g10*	43·00	55·3	8·37	676	156	1·2	1910	2490	205	726	94	18	68	7	34	6·3	14	1·8	12	1·9	10	61	18	0·67	12·69
1-sp03h09	44·70	55·0	9·35	666	194	1·2	2190	2750	249	891	119	21	82	9	41	7·8	18	2·2	14	2·1	10	80	23	0·63	11·49
1-sp03h13	46·60	55·0	12·80	653	198	1·3	1860	2820	291	1030	134	17	88	10	44	7·5	18	2·0	10	1·6	9	82	24	0·47	8·67
2-ap04g04	45·40	55·9	8·34	665	68	0·4	880	1060	82·5	274	33·1	8	24	2	11	2·3	6	0·8	5	0·9	8	40	21	0·90	16·60
2-ap04g06*	44·40	55·5	9·28	687	74·8	0·4	993	1280	98·7	333	42·2	9	30	3	14	2·9	7	0·9	6	1·0	9	46	15	0·77	14·69
2-ap04g08*	46·90	55·4	9·84	619	89·4	0·5	1080	1390	116	390	50·5	11	32	3	18	3·0	8	1·0	7	1·2	8	52	22	0·81	13·35
2-sp03h04	45·80	55·0	9·20	681	75·1	0·4	968	1130	90·7	303	37·8	8	27	3	14	2·6	6	0·9	6	1·0	8	51	20	0·80	15·99
2-sp03h11	45·30	55·0	9·15	735	84·7	0·4	1120	1400	117	396	47·6	10	33	4	16	3·1	8	0·9	6	1·0	8	50	15	0·77	14·69
2-sp03h14	43·30	55·0	9·34	700	103	0·6	1300	1620	133	464	57·6	12	39	4	20	3·7	8	1·1	7	1·3	10	75	21	0·76	14·09
2-sp03h05	43·00	55·0	9·25	634	77·9	0·4	955	1170	90·8	310	39·2	10	26	3	14	2·7	7	0·8	7	1·0	8	54	20	0·94	15·21
2-sp03h07	43·70	55·0	8·65	627	79	0·4	985	1230	97·4	326	38·8	10	27	3	14	2·8	7	0·9	6	1·0	8	54	18	0·93	15·85
SR2 sample—appinite																									
1-ap04a12*	42·10	55·5	23·50	1360	109	7·3	904	1340	112	404	50·5	13	39	4	19	3·7	9	1·2	8	1·3	8	38	15	0·90	11·18
1-ap04a14	42·60	55·1	20·00	1350	228	4·2	1410	2310	213	857	127	22	94	10	46	8·2	20	2·4	16	2·3	9	54	28	0·62	6·93
SR2 sample—appinite (suite)																									
1-sp01b07	42·60	55·0	24·60	1340	200	5·8	1190	2090	232	897	126	22	81	9	42	7·8	19	2·3	13	2·1	8	39	11	0·66	5·90
1-sp01b08	42·30	55·0	15·70	1270	218	2·2	1050	1900	219	891	132	18	88	10	45	8·4	18	2·3	14	2·1	7	40	11	0·50	4·97
1-sp05f08	42·50	55·0	23·00	1320	242	8·3	1330	2440	261	1060	152	22	99	11	50	9·1	21	2·7	17	2·3	8	31	12	0·53	5·46
1-sp05f09	42·90	55·0	18·10	1310	240	5·1	1250	2230	249	1010	148	20	101	10	51	9·1	22	2·5	16	2·4	8	47	17	0·51	5·27
R-ap04a08	41·30	55·4	6·38	1490	132	0·6	947	1510	148	557	77·9	16	52	6	28	4·9	12	1·3	10	1·3	10	53	23	0·74	7·59
R-ap04a13*	44·70	55·3	20·30	1340	96·2	2·3	805	1100	96·3	348	45·1	11	32	4	18	3·4	9	1·1	7	1·1	9	55	19	0·89	11·15
R-sp01b06	43·60	55·0	23·50	1330	124	8·2	890	1200	115	429	60·1	12	45	5	23	4·6	12	1·6	10	1·6	7	30	8	0·71	9·25
R-sp05f03	47·20	55·0	12·10	1230	123	1·5	927	1280	120	445	61·4	14	44	5	24	4·6	12	1·3	9	1·5	7	47	20	0·80	9·43
SR3 sample—granitoid																									
1-ap04e12	43·30	54·8	9·44	600	165	1·3	2070	2750	219	735	95·4	21	71	7	35	6·7	16	1·9	13	2·0	10	93	34	0·76	13·55
1-ap04e13	52·00	54·6	9·44	714	195	1·5	2580	3370	270	878	113	22	79	9	40	7·3	18	2·2	14	2·5	11	95	29	0·72	14·26
1-ap04e14*	43·50	54·7	9·04	728	176	1·3	2420	3130	249	824	101	21	74	7	36	6·7	16	1·9	13	2·0	9	81	22	0·73	14·96
1-sp01d13	46·20	54·8	10·10	742	186	1·4	1980	2810	261	950	129	20	86	9	42	7·8	18	2·0	13	2·0	9	69	21	0·57	9·58
2-ap04f04*	44·70	55·2	8·22	643	75·2	<0·30	946	1170	91·1	304	37·1	9	26	3	12	2·7	6	0·8	5	0·9	8	40	25	0·84	15·92
2-sp01c07	47·40	54·8	8·84	665	76·6	0·3	1020	1230	94·4	324	38·2	10	26	3	14	2·8	7	0·9	5	1·0	8	49	19	0·92	16·67
2-sp01d06	45·40	54·8	0·95	654	47·9	<0·11	664	806	67·3	228	28·5	5	22	2	9	1·8	4	0·5	3	0·5	6	8	4	0·68	14·55

Rogart samples: 1, core compositions; 2, oscillatory rim; 3, unzoned rim. Strontian samples: 1, core or all crystal composition; 2, rim composition. R, bright rims present in the appinite apatite crystals. P_2O_5 and CaO are reported in wt % and the other elements in ppm.
*Analyses plotted in Fig. 3.
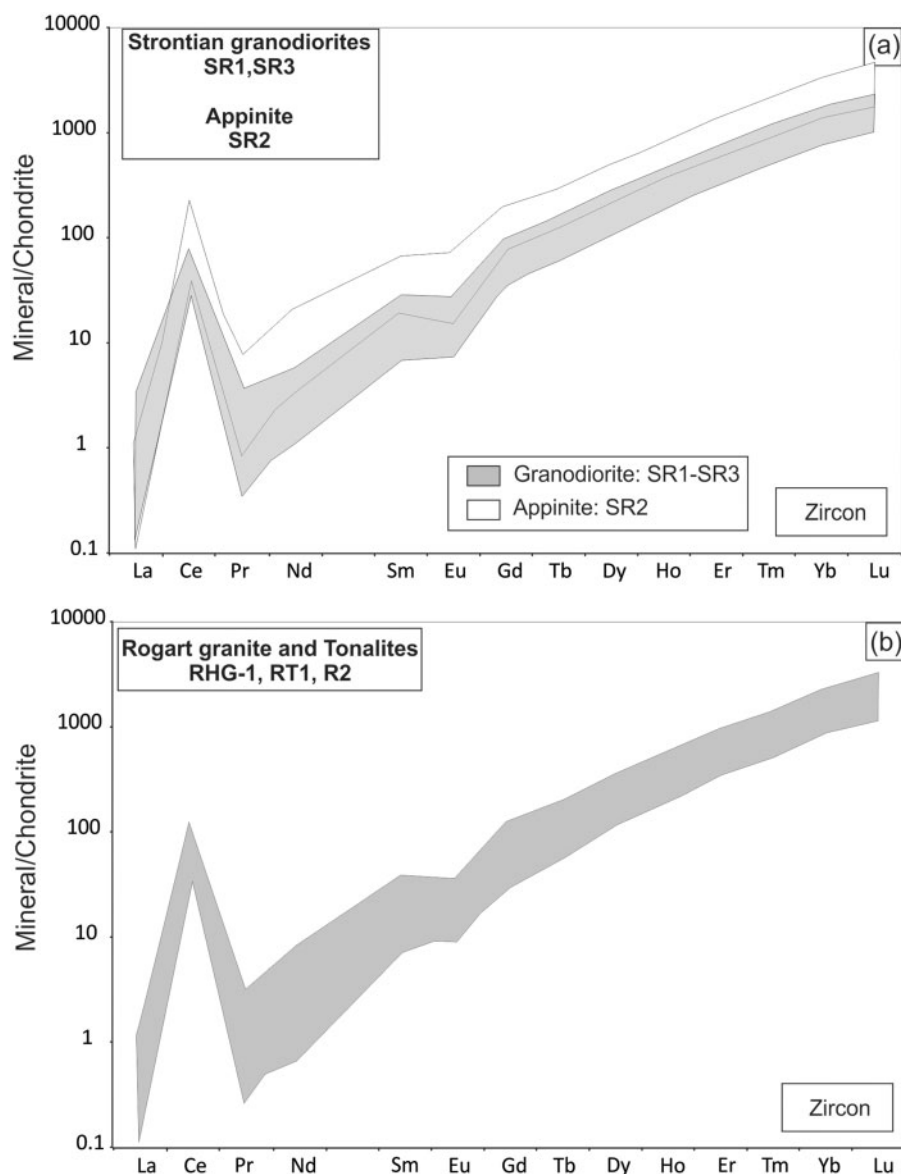
Fig. 10. Chondrite-normalized REE patterns for zircons in (a) Strontian granodiorites (SR1, SR3) and appinite (SR2). (b) Rogart granite (RHG-1) and tonalites (RT1, R2). (See Table 4 and Supplementary Data: Electronic Appendix 4.)

(appinite) samples. REE patterns (Fig. 10) support the suggestion that such zircons seem to have crystallized from REE-enriched melt pockets.

The granitoids: in situ *crystal fractionation and a late mixing event?*

In the Strontian granitoids, both apatite and titanite exhibit two chemical groups, which presumably relate to the same petrogenetic events. The first group (crystal cores) has higher REE contents and a more significant negative Eu anomaly. The second group (crystal rims) has a lower REE content, with a slightly negative to absent Eu anomaly.

Cores of titanite and apatite in Strontian record a systematic outward decrease in trace elements (Figs 6a, 7a, b, 9a, c and 11). For example, Fig. 7b shows a correlation between Zr and Y content, of which the latter can be used as a proxy for the HREE, which are compatible in titanite. The progressive decrease of Y is consistent with *in situ* crystal fractionation, as titanite and other accessory minerals progressively deplete the remaining melt in trace elements. The same systematics is observed in apatite cores (Fig. 9a–c), suggesting that the cores of titanite and apatite grew during the same interval.

However, progressive *in situ* crystal fractionation cannot explain the sudden compositional change observed in the

Table 4: *Analyses of zircon compositions (for full dataset see Supplementary Data)*

	SiO₂	P₂O₅	Sc	Y	Nb	La	Ce	Pr	Nd	Sm	Eu	Gd	Tb	Dy	Ho	Er	Tm	Yb	Lu	Hf	Ta	Pb	Th	U	Th/U
RT1 sample																									
2-ap05c05	33·2	0·028	97	550	2·94	–	39	0·052	1·1	2·11	0·80	10·9	3·22	43·2	16·8	88·1	21·1	228	49·8	9250	0·95	8·4	193	360	0·5
2-ap06c06*	33·3	0·035	98	503	2·45	–	41	0·067	1·2	2·04	0·78	10·4	3·16	39·7	15·6	80·8	19·0	198	43·8	8450	0·88	9·0	192	313	0·6
2-ap06c07	33·5	0·032	99	418	2·60	0·061	34	–	0·8	1·63	0·75	8·5	2·58	34·5	12·6	67·7	15·7	166	35·5	9420	0·85	8·0	191	327	0·6
2-oc03f04*	33·2	0·033	88	440	2·02	0·090	40	0·064	1·4	1·95	0·71	9·4	2·75	36·2	13·8	68·2	16·2	170	34·6	8710	0·78	9·7	225	315	0·7
2-oc03f05	33·3	0·061	85	394	1·91	0·158	32	0·103	1·0	1·57	0·69	8·4	2·58	32·0	12·4	62·1	15·1	154	32·1	9370	0·72	7·9	176	316	0·6
3-ap06c10	33·3	0·035	101	483	2·60	0·049	39	0·084	1·0	2·09	0·80	10·1	2·91	38·4	14·6	74·8	18·3	189	41·3	9040	0·87	10·6	241	398	0·6
3-oc03e14	33·2	0·029	98	560	2·58	0·047	34	0·048	1·3	2·04	0·66	10·7	3·13	43·6	17·3	87·9	23·4	242	51·3	9090	0·96	6·6	162	300	0·5
RHG-1 sample																									
1-ap05d04	33·2	0·0375	93	542	2·73	0·233	36·7	0·123	1·16	1·59	0·84	10·9	3·27	42·9	16·9	86·6	21·4	227	48·7	8510	1·03	9·21	189	349	0·5
1-oc03d05	33·2	0·0453	98	591	2·99	0·289	53·7	0·182	1·58	3·07	0·883	15·3	3·96	48·4	18·4	95·9	22·2	240	46·8	9560	1·13	12·7	325	421	0·8
1-oc03d07	33·2	0·0384	107	869	3·58	0·140	60·5	0·27	2·87	5·1	1·59	20·1	5·83	73·5	27·8	136	31·7	330	66·6	9170	1·19	15·8	388	491	0·8
2-ap05f07	33	0·034	81	379	2·27	0·064	30·2	0·0509	0·767	1·57	0·578	7·54	2·35	30	11·5	58·6	13·9	146	31·6	9430	0·738	8·18	175	328	0·5
2-oc03e04	33·2	0·0258	109	593	2·8	0·078	43·3	0·0686	1·02	2·37	0·807	11·2	3·6	48·2	18·9	93	23·3	244	48·6	10700	1·16	10·3	276	437	0·6
2-oc03e08*	33·2	0·0315	85	480	2·14	0·098	33·4	0·0815	0·871	1·52	0·686	8·75	3·08	36·6	14·8	76·7	18·2	189	39·3	8640	0·964	8·36	200	331	0·6
2-oc03e09*	33·2	0·0342	100	611	3·36	0·082	44·3	0·11	1·09	2·44	0·884	10·6	3·65	48·6	18·5	96·7	23·6	247	52·4	8700	1·16	9·2	208	302	0·7
3-ap05d06	32·9	0·0326	78	385	1·96	0·260	31·7	0·106	1·11	1·46	0·606	8·79	2·4	31·1	12	62·2	14·7	150	32·5	8410	0·773	11·6	199	346	0·6
R2 sample																									
1-ap05f12*	33·2	0·034	90	581	3·6	0·064	48	0·083	1·4	2·0	1·05	11	3·5	44	17	92	22	231	51	9050	1·04	11·5	236	368	0·6
1-oc03b07	33·2	0·041	115	584	1·7	0·071	32	0·133	1·6	3·2	1·01	13	4·1	50	19	93	21	222	44	8140	0·63	7·1	160	222	0·7
2-ap05f11	33·3	0·043	94	649	3·2	–	52	0·109	1·6	3·1	1·22	15	4·2	52	20	101	24	241	52	8380	0·96	13·7	280	379	0·7
2-oc03b11	33·2	0·028	90	403	2·0	–	33	0·057	1·1	1·7	0·65	9	2·5	33	13	65	16	161	34	9280	0·81	8·9	202	364	0·6
2-oc03c04	33·2	0·022	110	593	3·0	0·132	38	0·041	1·0	1·8	0·75	11	3·4	45	18	93	24	248	53	9260	0·92	9·7	223	429	0·5
SR1 sample																									
1-oc03f06	33	0·034	91	471	2·0	0·031	30	0·055	0·85	1·6	0·69	9	2·8	38	15	74	17	190	38·2	8320	1·12	7·6	179	313	0·6
1-oc03f09	33	0·032	90	708	1·0	0·735	36	0·318	2·57	4·0	1·47	19	5·2	64	22	108	25	240	48·8	8580	0·65	12·2	265	338	0·8
2-ap06c14*	33·3	0·034	110	537	2·2	–	43	0·041	0·71	1·7	0·79	10	3·4	43	16	83	19	197	43·6	8700	1·17	13·0	324	466	0·7
2-ap06d04*	33·1	0·030	96	447	2·1	0·072	30	0·054	0·94	1·8	0·72	10	2·7	33	14	68	17	178	40·1	7980	1·06	7·5	160	281	0·6
2-ap06d10	33	0·035	104	511	2·6	–	34	<0·0297	0·91	1·6	0·64	9	3·3	39	16	81	20	207	45·8	8220	1·25	9·3	207	377	0·5

(continued)

Table 4: *Continued*

	SiO₂	P₂O₅	Sc	Y	Nb	La	Ce	Pr	Nd	Sm	Eu	Gd	Tb	Dy	Ho	Er	Tm	Yb	Lu	Hf	Ta	Pb	Th	U	Th/U
SR2 sample																									
1-ap06d13*	33·1	0·038	111	676	2·2	0·026	34	0·12	2·0	3·1	0·98	17	4·8	59	22	102	24	238	49	9320	0·97	10	236	334	0·7
1-oc04b10	33	0·072	116	1230	3·8	–	74	0·25	3·4	5·5	2·82	29	8·4	109	41	202	49	480	99	9610	1·53	60	1230	1340	0·9
2-oc04a07	33	0·061	117	1080	4·5	–	105	0·24	4·1	6·5	2·97	31	8·9	101	35	167	37	362	73	9170	2·08	123	2690	1780	1·5
2-oc04b07	33	0·064	108	1110	5·2	0·077	114	0·30	4·3	6·4	3·19	32	8·9	103	36	166	38	364	71	9170	2·39	177	3520	2240	1·6
3-oc04b05	33·2	0·038	100	932	1·1	0·249	39	0·54	7·2	7·5	3·01	26	7·6	84	30	143	34	332	66	8770	0·69	32	712	601	1·2
3-oc04b11	33	0·030	99	818	3·2	–	66	0·15	2·2	4·5	1·78	19	5·7	71	26	128	30	307	67	11000	1·64	56	1160	2170	0·5
3-oc04b12	33	0·057	135	1270	5·4	0·099	91	0·26	3·8	5·4	2·28	27	7·8	103	41	208	50	502	101	8390	2·19	64	1320	1260	1·0
SR3 sample																									
1-ap06g05*	33·1	0·024	93	433	2·3	0·059	33	0·05	0·66	1·4	0·80	8·3	2·9	35	14	69	17	173	35	8010	0·91	9·3	219	359	0·6
1-oc03a06	33	0·037	121	724	2·9	0·068	42	0·12	1·87	2·9	1·07	14·5	4·6	60	23	111	27	265	55	8600	1·28	14·8	380	530	0·7
2-ap06g08	33·2	0·036	94	397	2·4	0·087	30	0·09	0·74	1·9	0·57	8·2	2·3	31	12	63	15	157	33	7790	0·80	8·2	185	327	0·6
2-ap06g09	33	0·038	87	349	1·9	0·081	30	0·06	0·84	1·4	0·64	7·7	2·2	28	11	54	13	131	27	7010	0·80	9·7	211	340	0·6
2-oc03b04	33	0·032	96	441	2·0	0·077	28	0·04	0·92	1·6	0·59	7·4	2·6	34	13	68	17	180	38	7500	1·01	7·8	158	278	0·6
3-oc03a05	33	0·035	112	514	2·1	0·055	39	0·09	0·88	1·9	0·84	9·9	3·2	41	16	76	19	194	40	8220	1·04	13·5	328	439	0·7
3-oc04d05	33	0·043	87	629	1·0	0·502	32	0·22	2·29	3·7	1·09	15·5	4·8	57	20	95	24	230	48	8100	0·73	11·1	244	326	0·7

1, 2 and 3 correspond to analyses from cores (1) towards external rims (3). SiO₂ and P₂O₅ are reported in wt % and the other elements in ppm.
*Analyses plotted in Fig. 4.
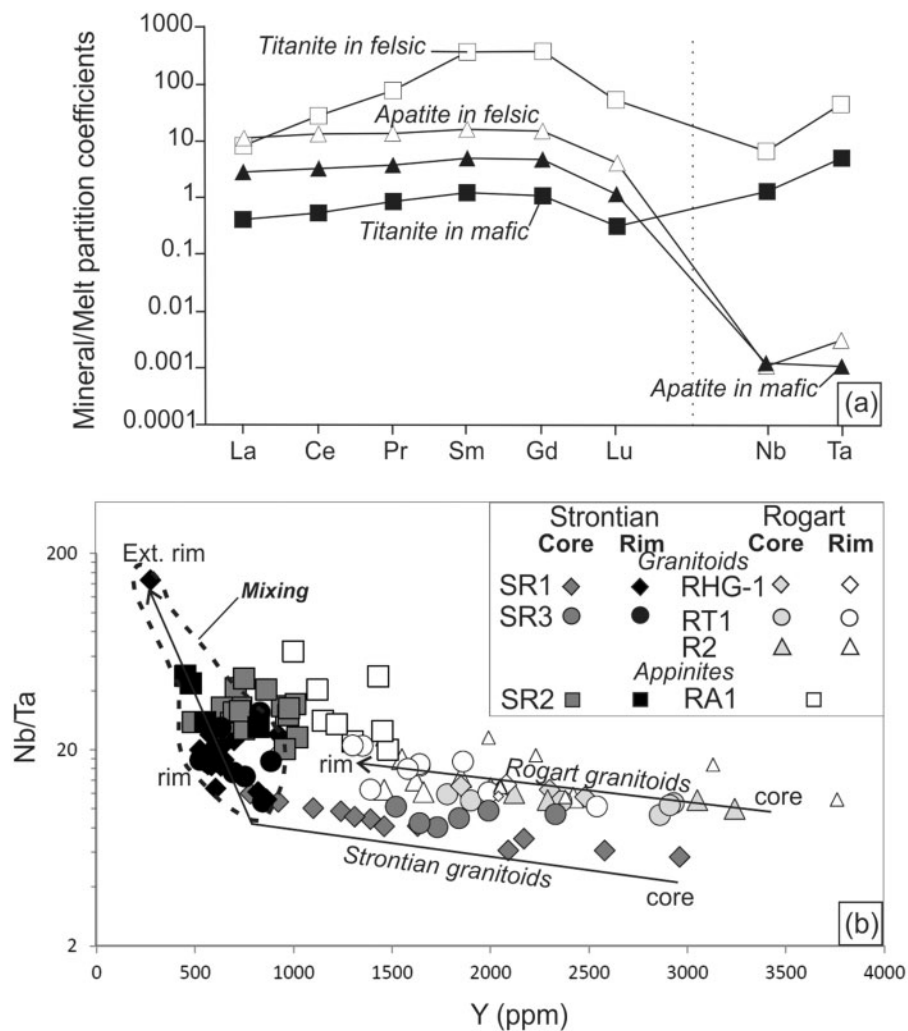
Fig. 11. (a) Selected mineral–melt partition coefficient for apatite and titanite for felsic and mafic melt compositions (from Prowatke & Klemme, 2005, 2006). (b) Nb/Ta versus Y (ppm) for titanites from the Strontian and Rogart localities. A sudden increase of Nb/Ta recorded in titanite rims in Strontian granitoids indicates a mixing event with a mafic magma (field defined by dashed borders).

titanite and apatite rims in Strontian (Figs 6a, 7a, b, 9c, d and 11). There are several possible causes, such as a change in oxygen fugacity, fluid circulation–hydrothermal alteration or magma composition (e.g. Piccoli *et al.*, 2000; Prowatke & Klemme, 2005, 2006; Smith *et al.*, 2009; McLeod *et al.*, 2011). More reducing magma conditions will lead to the dissolution of the outer rims of titanite crystals, resulting in the stabilization of ilmenite within titanite and the regrowth of titanite with a lower REE content (e.g. Piccoli *et al.*, 2000; McLeod *et al.*, 2011). Although the presence of titanite–magnetite–quartz in a felsic magma indicates relatively high $f\mathrm{O}_2$, decreasing $f\mathrm{O}_2$ in such a magma has been shown to induce crystallization of ilmenite (Wones, 1989). Moreover, under reduced conditions, the lower activity of ferric iron induces the need to charge balance REE in the titanite structure, which can partly explain the lower REE uptake. Except for the

change in REE content, other features that might characterize a change in $f\mathrm{O}_2$ are not observed in the Strontian titanites. Belousova *et al.* (2002a) have shown that La/Sm, Ce/Th and Y/ΣREE in apatite compositions are dependent upon the oxygen fugacity of the magma. La/Sm and Ce/Th increase with $f\mathrm{O}_2$, whereas Y/ΣREE tends to decrease. None of these ratios show systematic differences between apatite cores and rims in the samples discussed here (Table 2; Supplementary Data: Electronic Appendix 2). It is therefore unlikely that abrupt changes in REE between the cores and rims of apatite or titanite can be explained by a simple change in $f\mathrm{O}_2$. Hydrothermal alteration of titanite is characterized by patchy zoning and formation of anhedral crystals with trace element contents depending on the nature and chemistry of the fluid (e.g. Piccoli *et al.*, 2000; Horie *et al.*, 2008; Smith *et al.*, 2009; McLeod *et al.*, 2011). Titanites from the Strontian granitoids are euhedral

and have typical magmatic zoning and do not reveal obvious hydrothermal alteration between cores and rims (Fig. 2a and b). Prowatke & Klemme (2005) have shown that $D_{\text{titanite/melt}}$ for the REE and some other trace elements (Ta, Nb) is strongly influenced by melt composition (Fig. 11a). They have shown that $D_{\text{titanite/melt}}$ increases significantly for these elements from mafic to felsic magma compositions. For instance, Gd $D_{\text{titanite/melt}}$ varies from about unity in mafic compositions to 370 in the most felsic compositions studied. Our results show major systematic changes for the same elements (REE, Ta, Nb) between cores and rims, with the rim values plotting within the field for appinites (Table 2; Supplementary Data: Electronic Appendix 2; Figs 5a and 6a, b). Another example is illustrated in Fig. 11b based on the Nb/Ta ratio in titanite. In this figure, Nb/Ta ratios in Strontian titanites increase significantly towards those in the appinite and in the titanite rims of the granitoids. This phenomenon can be best explained by considering the $D_{\text{titanite/melt}}$ for Nb and Ta (Fig. 11a). Indeed, $D_{\text{Nb}}/D_{\text{Ta}}$ felsic $\ll D_{\text{Nb}}/D_{\text{Ta}}$ mafic is mimiced by the Ta/Nb ratio in titanite. Prowatke & Klemme (2006) have shown that $D_{\text{apatite/melt}}$ increases from mafic towards felsic melt compositions for the REE. The apatites from our study reveal changes in REE composition between cores and rims, but no systematic changes for the other trace elements. It therefore seems likely that the titanite and apatite rims in the Strontian granitoids record a mixing event with a more mafic magma, characterized in these minerals by (1) an abrupt decrease in REE in the rims of both minerals, (2) an abrupt decrease in Nb and Ta in titanite rims and (3) rim compositions comparable with appinite apatite or titanite compositions (Fig. 12b). This conclusion, at the micrometre scale, is consistent with numerous macro-scale mixing and mingling features between the granitoids and mafic magmas observed at the locality from which the samples were taken, including abundant microgranular mafic enclaves and a disrupted synplutonic microdiorite dyke.

In Rogart, titanite and apatite trace element contents decrease generally from the core towards the rim (Figs 7a, b, 8b and 9b, c). Unlike Strontian, there is no abrupt change in their chemistry at the rim, and the overall trends are consistent with progressive *in situ* crystallization of minerals that crystallized simultaneously (Fig. 12b). Petrographic description and some analyses have highlighted some dissolution–reprecipitation BSE-bright zones (Fig. 2e). When these zones were large enough to be analysed they were shown to be enriched in certain elements (e.g. HREE + Y and Nb, Figs 6b and 7b; Table 2; Supplementary Data: Electronic Appendix 2). These brighter zones are always succeeded by a zone that plots within the general core-to-rim trend of the Rogart titanite compositions [Figs 2e (e.g. a14), 6b and 7b]. Thus, these dissolution–reprecipitation episodes are thought to

be a consequence of injection of several pulses of the same magma, which is consistent with recent interpretations of the construction of the pluton (Kocks *et al.*, 2013).

The appinites: in situ *crystal fractionation?*

The petrogenetic interpretations of the appinite titanite and apatite compositions are somewhat different, as titanite is a late phase in sample SR2 (interstitial growth) and is anhedral–euhedral in sample RA1 (Fig. 2f and g). In Rogart, the titanite and apatite REE patterns are similar (flat LREE with an absent or slightly positive Eu anomaly; Figs 5c and 8c). This would imply that $D_{\text{apatite/melt}}$ and $D_{\text{titanite/melt}}$ for the different REE are comparable for a given magma composition and that the minerals crystallized at a similar time, consistent with the data of Prowatke & Klemme (2005, 2006) for mafic magma compositions. In contrast, the appinitic titanites and apatites from Strontian have rather different REE patterns and apatite cores and rims have distinctive REE contents (Fig. 9a and c; Supplementary Data: Electronic Appendices 2 and 3). It is also observed that apatite with BSE-bright rims is systematically present as inclusions in late phases such as interstitial titanite or amphibole (Fig. 3f), suggesting that apatite rim growth is synchronous with titanite. Changes in REE content between cores and rims in apatite may, therefore, be related to the late growth of titanite (Fig. 12a). Progressive depletion of the melt in LREE–MREE as a result of early apatite saturation may explain the difference in titanite REE patterns between appinites from Rogart and Strontian (Fig. 5c).

Summary of apatite–titanite crystallization history

Based upon the data and observations presented above, it is possible to reconstruct the different stages of growth of apatite and titanite and link them to pluton petrogenesis (Fig. 12a and b). For this purpose, the average (Sr/Sm) ratio is used in Fig. 12c because it allows discrimination of the nature of the magma from which the mineral has crystallized. The average Sr content in the cores or rims of the two minerals is homogeneous and correlates with the Sr whole-rock content (see below). Sm is used as it has been shown from experimental studies (Prowatke & Klemme, 2005, 2006) that titanite and apatite REE distribution coefficients vary significantly between mafic and felsic magma compositions. Bearing these points in mind, the following crystallization sequence for the granitoids is proposed.

(1) In the granitoids, inclusion of apatite within titanite and zircon demonstrates that apatite is an early phase in the crystallization sequence. The presence of apatite within titanite zones implies that apatite crystallized slightly earlier than or simultaneously with titanite. Most of the time, apatite inclusions do not appear within the FT zones that crystallized first in titanite. Moreover, both apatite and titanite have
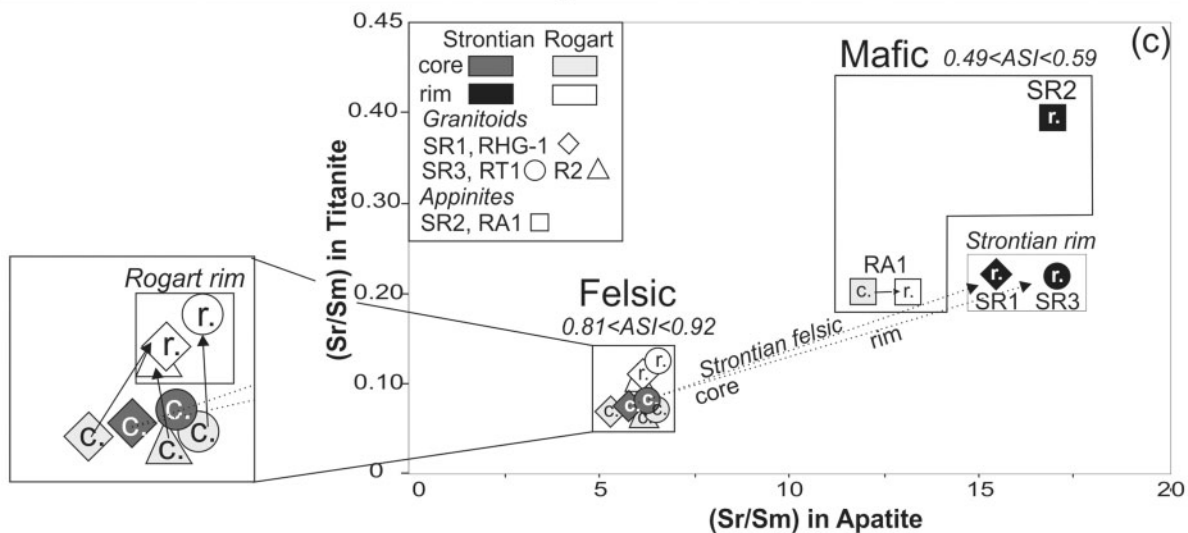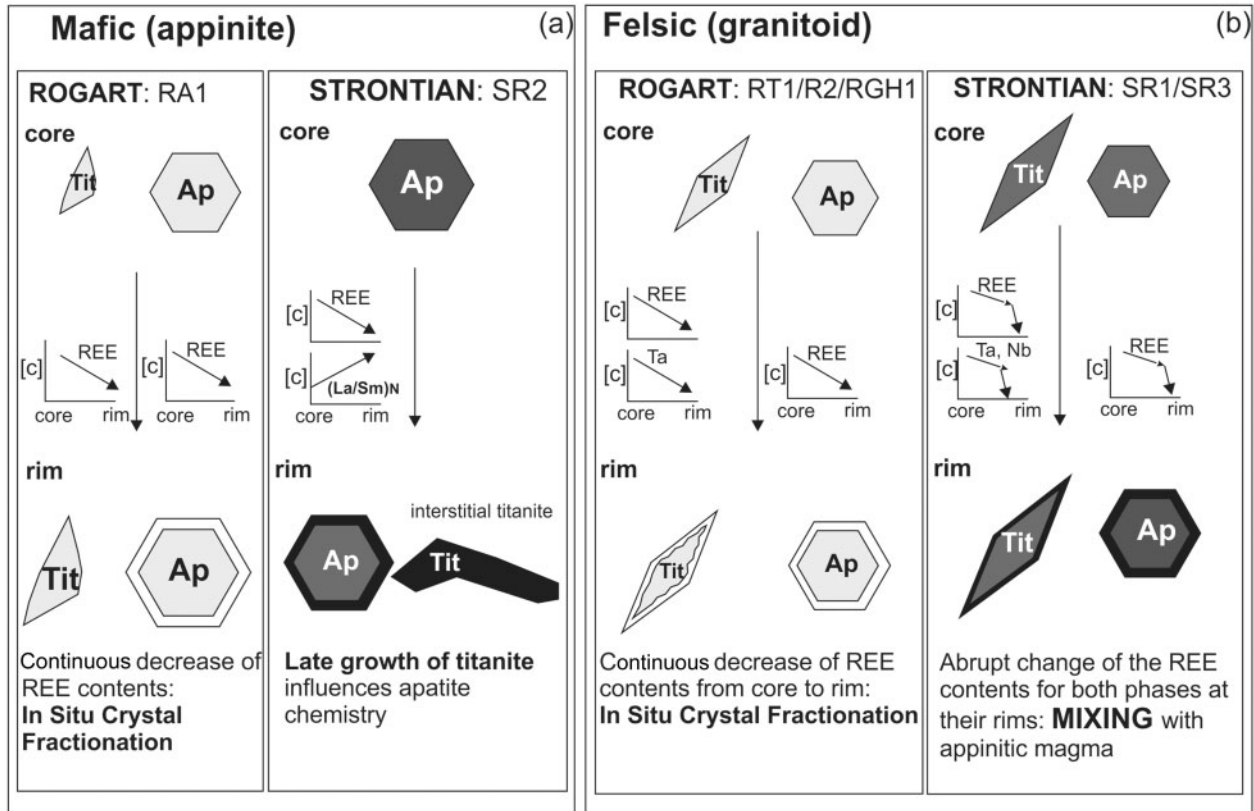
Fig. 12. (a, b) Summary of the crystallization history of titanite and apatite in the felsic and mafic intrusive rocks from Rogart and Strontian. (c) Discrimination of the host-rock composition (felsic vs mafic) based on the Sr/Sm ratio in apatite and titanite. Each sample point represents the average composition of core and rim (Supplementary Data: Electronic Appendices 2 and 3).

homogeneous cores with an abrupt change in REE composition at their rims. If titanite had crystallized later than apatite, a shift in apatite REE patterns owing to the new uptake of LREE–MREE by titanite might be expected (see Sr2 sample in Fig. 8c). This is not observed (Fig. 8). All these observations strongly

suggest that these minerals have crystallized simultaneously. In Fig. 12c, the Strontian and Rogart titanite and apatite core compositions plot in the same area.

(2) Subsequently, rims of both minerals within the different granitoids crystallized (Fig. 12b and c). The abrupt change in the composition of the rims of

Strontian samples is similar to the mafic samples in Sr/Sm space, revealing a mixing event between the granitoid and a mafic magma. On the other hand, Rogart granitoid rim data plot close to their core compositions. As a result of *in situ* crystal fractionation, the Sr/Sm ratio for both minerals increased slightly, but still clusters in a tight area (Fig. 12c).

For the appinite, the (Sr/Sm) ratio for each mineral is characteristically higher than for the granitoid and plots in an area where $(Sr/Sm)_{Apatite} >$10 and $(Sr/Sm)_{Titanite}$ $>$0·20. RA1 apatite and titanite grew simultaneously and have core and rim composition plotting in a tight field. Apatite cores in SR2 crystallized first, indicated by the increase of $(La/Sm)_N$ in apatite towards the rim and the interstitial habit of titanite crystals (Fig. 12a). Consequently, $(Sr/Sm)_{Titanite}$ for SR2 plots at a higher value in Fig. 12c.

Thus, the $(Sr/Sm)_{Apatite}$ versus $(Sr/Sm)_{Titanite}$ of a given sample can be used to track *in situ* crystallization and to discriminate the composition of the magma from which the accessory minerals crystallized (felsic or mafic). In this example, the plot identifies a mixing event in the petrogenesis of the Strontian granitoids, but further work on other samples and magma compositions needs to be done to assess if this kind of diagram can be used more widely as a discrimination tool. In this case, the diagram is only of use when combined with a detailed petrographic study. This contribution has shown that detailed study of accessory minerals can highlight petrogenetic processes not visible with whole-rock data only. However, whole-rock chemistry and isotope data (O, Nd, Sr) argue for petrogenetic processes that could not be observed in the apatite, titanite or zircon trace element chemistry; for example, metasediment assimilation (Fowler *et al.*, 2008). This is consistent with the bulk of such contamination occurring before crystallization of the accessory phases; that is, en route to the site of magma emplacement.

Accessory mineral records of whole-rock composition

Sr–V in apatite and titanite

$V_{apatite}$, $Sr_{titanite}$ and $Sr_{apatite}$ have significant potential to reflect the content of these elements in the whole-rock and therefore have potential applications for provenance studies. Previous studies have suggested a link between apatite composition and that of the whole-rock (e.g. Hoskin *et al.*, 2000; Belousova *et al.*, 2001, 2002*a*; Chu *et al.*, 2009; Jennings *et al.*, 2011; Miles *et al.*, 2013). From these studies, several correlations have been highlighted, such as Sr in apatite ($Sr_{apatite}$) reflecting the degree of fractionation of the host granite. Chu *et al.* (2009) have also used Sr, MnO and F contents in apatite to infer different settings of pluton genesis. In the Scottish samples studied here,

differences between the Sr contents of apatite cores and rims are minor (Fig. 13a, Table 3; Supplementary Data: Electronic Appendix 3), which is consistent with the work of Tepper & Kuehner (1999) suggesting that elements (Mn, Fe, Sr) occupying the Ca site in apatite are redistributed between zones by intracrystalline diffusion. A plot of $Sr_{apatite}$ versus Sr_{WR} defines two separate groups corresponding to whole-rock (WR) ultramafic and granitoid compositions (Fig. 13a). Literature data for granitoid samples have also been plotted (Hoskin *et al.*, 2000; Belousova *et al.*, 2002*a*; Chu *et al.*, 2009; Jennings *et al.*, 2011), which correspond well to our new data. 'Gabbros' from the suite of complex intrusive bodies studied by Jennings *et al.* (2011) also plot in the same field as the appinites (E. S. Jennings & H. R. Marschall, personal communication). The data distribution in Fig 13a therefore suggests that magma composition may have some influence on Sr partition coefficients, in contrast to the conclusions of Klemme & Prowatke (2005). Similarly, V content is fairly homogeneous in apatite crystals ($V_{apatite}$); Fig. 13b shows the relationship with V_{WR}. There is an increase of $V_{apatite}$ from felsic to ultramafic samples, again discriminating the two main compositions.

Although such apatite and whole-rock compositional correspondence has been investigated in recent years, the similar use of titanite has not. Figure 13c and d shows that Sr in titanite ($Sr_{titanite}$) correlates with $Sr_{apatite}$ and therefore with Sr_{WR}. There is a good correlation between the Sr content of apatite and titanite and there is a consistent enrichment factor of about 10 in apatite with respect to titanite (Fig. 13d). Available data from the literature (Hoskin *et al.*, 2000) plot on the same trend.

Figure 14a and b demonstrates that Sr_{WR} and V_{WR} reflect the degree of fractionation of the samples, although the Sr data are rather more scattered (Fig. 14a and b). Reported SiO_{2WR}–$Sr_{apatite}$ values for the felsic samples are consistent with available literature data (Hoskin *et al.*, 2000; Belousova *et al.*, 2002*a*; Chu *et al.*, 2009; Jennings *et al.*, 2011), although in general our samples have higher $Sr_{apatite}$ for similar SiO_2 values (Fig. 14c). This can be explained by the characteristic high Ba–Sr contents of our samples (Fowler *et al.*, 2001, 2008). Comparable ultramafic compositions (E. S. Jennings & H. R. Marschall, personal data) and our appinitic samples (Fig. 14c) define a second trend (see above, Fig. 13a). Similarly, $Sr_{titanite}$ (Fig. 14d) and $V_{apatite}$ (Fig. 14e) show similar trends. In summary, $Sr_{apatite}$, $Sr_{titanite}$ and $V_{apatite}$ seem to reflect the degree of fractionation of the Strontian and Rogart samples.

### Apatite and titanite: recovery of whole-rock REE content

Application of distribution coefficients to early crystallizing apatite and titanite should allow recovery of the original melt composition. Zircon was not tested because previous workers have shown that back-calculation for this mineral is difficult, either because of substitution by
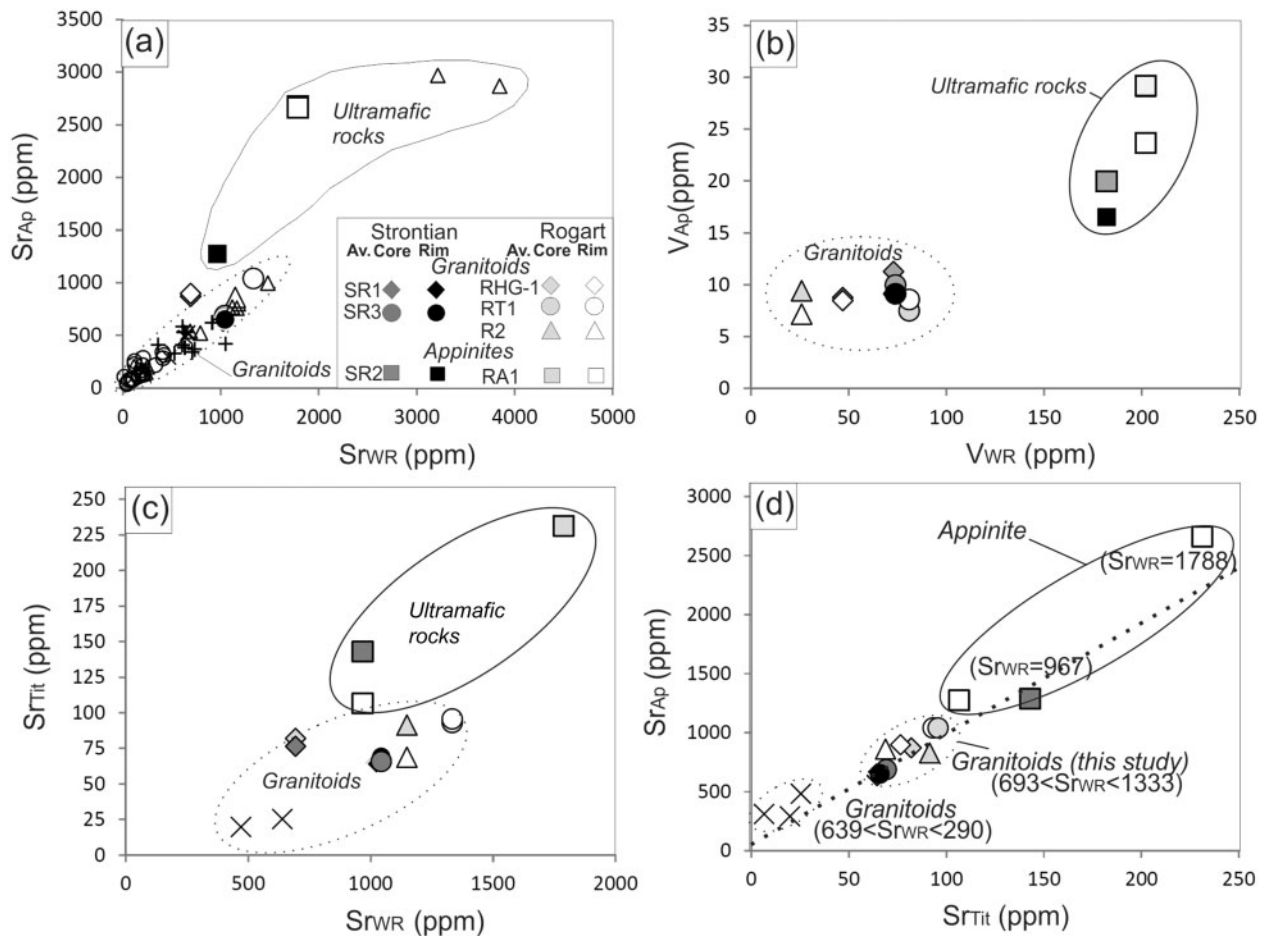
Fig. 13. Variation of Sr and V content in apatite (a, b) and titanite (c) versus whole-rock (WR) composition (Fowler *et al.*, 2001, 2008). Average compositions of cores and rims are plotted for each sample (See Supplementary Data: Electronic Appendices 2 and 3). (a) Average apatite values from Hoskin *et al.* (2000, cross symbols), Belousova *et al.* (2002a, small open circles); Chu *et al.* (2009, plus symbols); Jennings *et al.* (2011) and E. S. Jennings & H. R. Marschall (personal communication; small open triangles) are also shown. (c, d) Data from Hoskin *et al.* (2000, cross symbols) are also plotted. (d) Sr_{Ap} versus Sr_{Tit} for the Rogart and Strontian samples. The dotted line represents a 1:10 correlation between Sr contents in apatite and titanite.

xenotime (e.g. Hoskin *et al.*, 2000) or because of the lack of experimental data for our felsic range of magma compositions. Strontian samples have been affected by a mixing event (see discussion above) and therefore cannot be used to calculate original whole-rock values. We therefore test the back-calculation approach on Rogart titanite and apatite, which have fairly homogeneous compositions. In a first stage, calculations for felsic samples were done using available K_D values from experimental studies for both minerals (e.g. Tiepolo *et al.*, 2002; Prowatke & Klemme, 2005, 2006), giving results that appear to be completely inconsistent (especially for titanite) with the whole-rock data (Supplementary Data: Electronic Appendix 5). Compositions used during the experiments are dissimilar to the composition of our samples. Therefore, apatite and titanite K_D values were chosen from natural samples (mineral or glass; Luhr *et al.*, 1984) with a bulk composition that is more appropriate. Results calculated with apatite

and titanite core compositions from the RHG-1 and RT1 samples show reassuring comparability with the whole-rock chondrite-normalized REE patterns (Fig. 15a and b; Fowler *et al.*, 2001; Table 4 and Supplementary Data: Electronic Appendix 4). Calculations for sample R2 give a similar pattern shape but systematically higher REE contents than the whole-rock data (Fig. 15c). Apatite gives more reliable results than titanite but calculated HREE abundances for both minerals plot far above the whole-rock data. This cannot be explained by later saturation of zircon in which the HREE are extremely compatible because apatite crystals have been found as inclusions parallel to zircon growth zones, implying that they grew at the same time. R2 apatites systematically have lower La/Sm and higher Y/(ΣREE) than the other samples (Table 4; Supplementary Data: Electronic Appendix 4), which could suggest a different fO_2 for this sample (Belousova *et al.*, 2002a), although there is a lack of experimental data
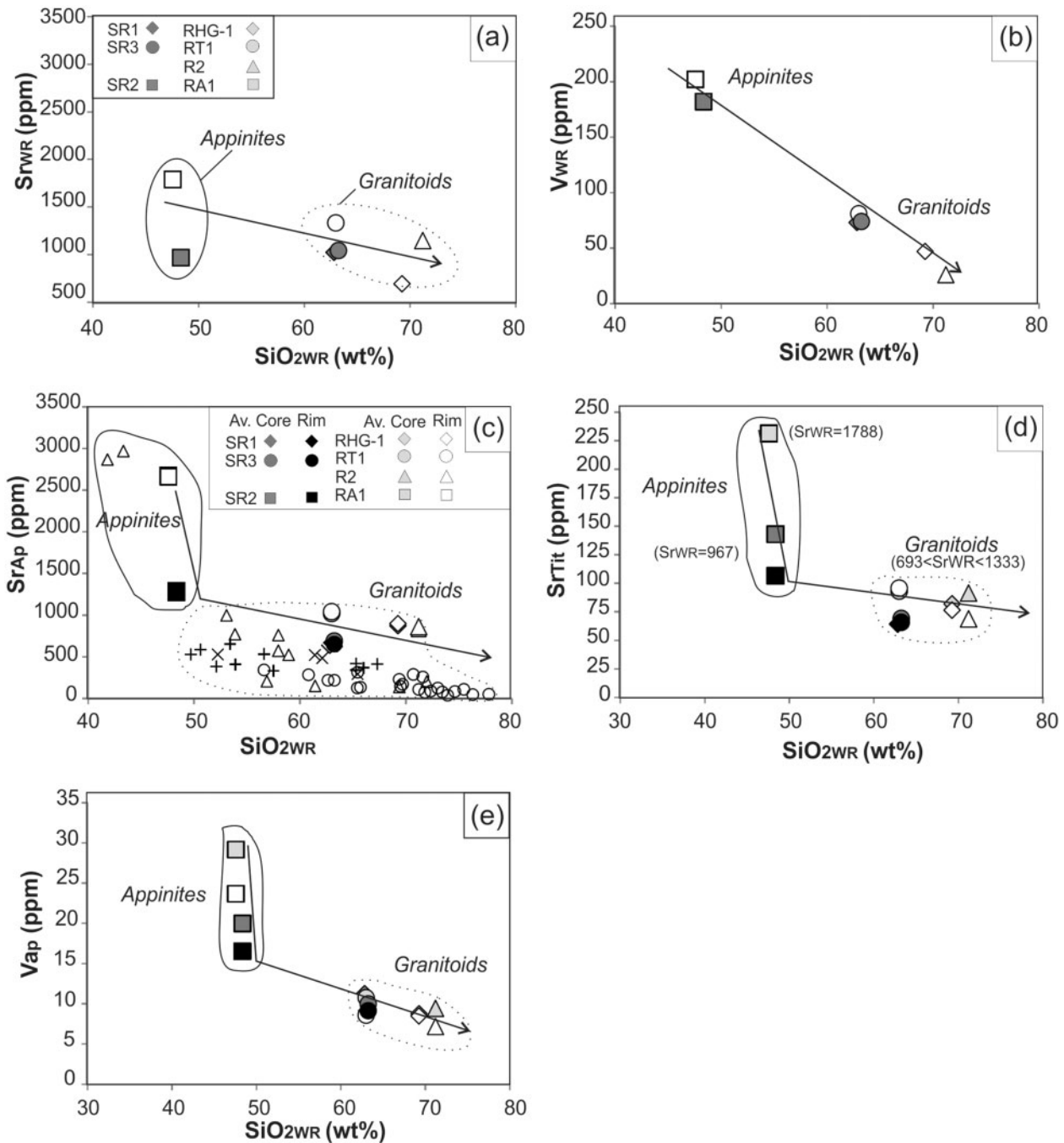
Fig. 14. (a, b) Variation of whole-rock Sr and V content versus SiO_2 for the samples studied. Data from Fowler *et al.* (2001, 2008). (c, e) Variation of Sr (ppm) and V (ppm) content in apatite versus SiO_{2WR}. (d) Variation of Sr (ppm) content in titanite versus SiO_{2WR}. The abundances of these elements within apatite and titanite vary with SiO_{2WR} content and reflect the degree of differentiation of the samples. (c) Literature data have also been plotted. (See Fig. 13 for data sources and symbols.)

to confirm this. Further, in plutonic igneous rocks such as these, it is entirely possible that the whole-rock itself does not represent a melt composition. Each sample is a combination of evolving melt and entrained crystals, such that for sample R2 admixture of a low HREE mineral (e.g. feldspar) would effectively reduce the whole-rock HREE content. The observed mismatch might therefore be related to different fO_2 conditions, to dissimilarity to the apatite compositions of Luhr *et al.* (1984), or to a difference in composition between the whole-rock composition and the evolving magma as recorded in the accessory minerals.
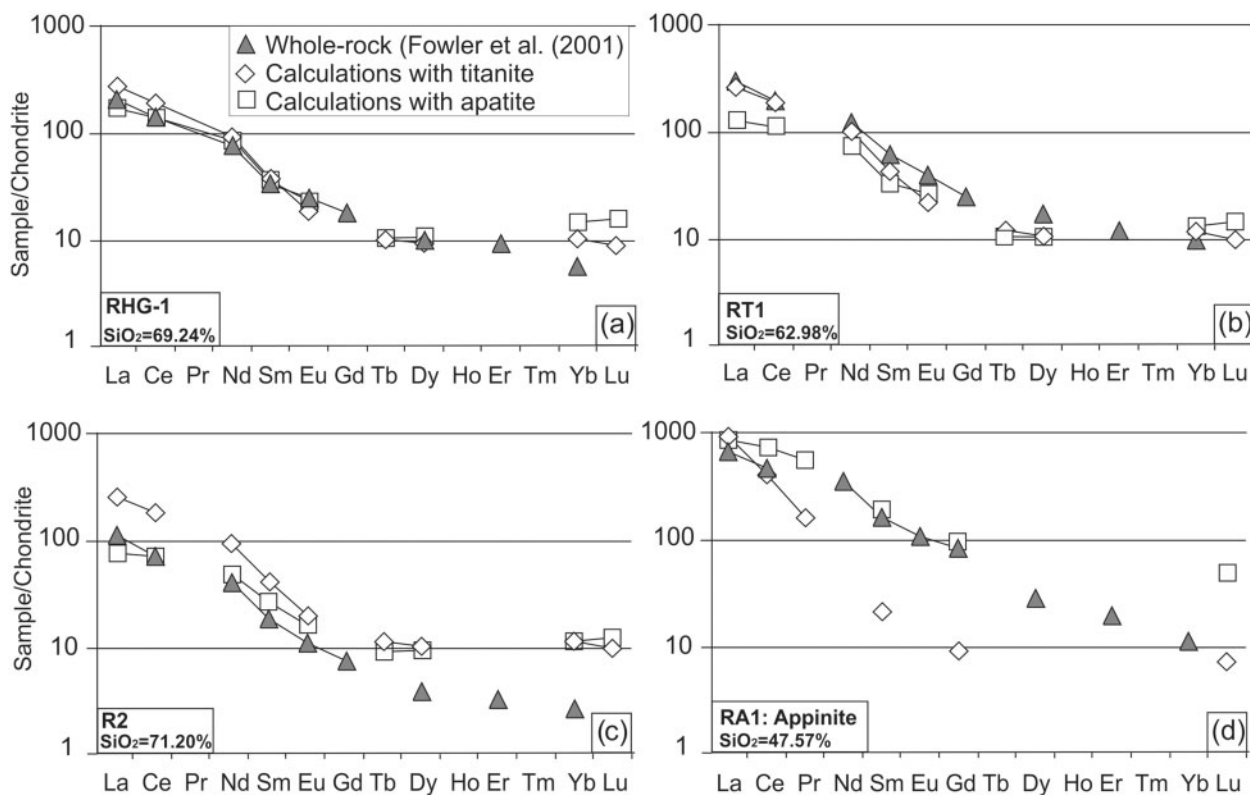
Fig. 15. Chondrite-normalized REE patterns modelled by back-calculating whole-rock compositions from titanite and apatite average core compositions in the Rogart samples (Supplementary Data: Electronic Appendices 2 and 3). Calculations were performed using $D_{apatite/melt}$ and $D_{titanite/melt}$ values from Luhr *et al.* (1984) for granitoids (a–c) and from Prowatke & Klemme (2005, 2006) for appinite (d). Data sources: Supplementary Data: Electronic Appendix 5. X-ray fluorescence whole-rock data are from Fowler *et al.* (2001) for the same samples.

For the Rogart appinite, K_D values for basic rocks are taken from Prowatke & Klemme (2006) (Table 4; Supplementary Data: Electronic Appendix 4). Calculations using apatite, which crystallized early in RA1 (Fig. 15d), have LREE concentrations consistent with the whole-rock data. Those performed with titanite, which is a late crystallizing phase, do not reflect the whole-rock data (Fig. 15d). The lack of experimental data for HREE distribution coefficients does not allow for comparison with the HREE.

What about zircons?

Zircon is undoubtedly one of the most widely used mineral to date rocks (e.g. Compston *et al.*, 1984; Feng *et al.*, 1993; Kosler & Sylvester, 2003, and references therein), and is extremely valuable for provenance studies (e.g. Fedo, 2000), to track magma sources (using O and Hf isotopes; e.g. Hawkesworth & Kemp, 2006; Dhuime *et al.*, 2012) and potentially to estimate oxygen fugacity (e.g. Ballard *et al.*, 2002; Trail *et al.*, 2011; Burnham & Berry, 2012). Some researchers (e.g. Heaman *et al.*, 1990; Belousova *et al.*, 2002*b*) have tried to discriminate source rock type using trace elements in zircons but the systematics remains unclear (see Hoskin & Schaltegger, 2003). The use of trace elements in a single grain of zircon to record petrogenetic

processes has been described as unsuccessful (e.g. Hoskin *et al.*, 2000), but a recent study by Gagnevin *et al.* (2010) suggested that U–Th–Y variations in zircon could reflect a magma mixing event. No significant elemental differences have been found within the zircon analytical data produced for this study. The only noticeable difference is the higher REE content of the appinite sample compared with the granitoids, which is suggested to be the consequence of late crystallization from REE-enriched melt pockets. Therefore, zircon seems not to be a good candidate to track petrogenetic processes.

CONCLUSIONS

Careful imaging and chemical characterization of single grain accessory phases (apatite and titanite) can be a powerful petrogenetic tool. With the new results presented here, several observations can be made, as follows.

(1) Apatite and titanite trace element data can be used to constrain part of the petrogenetic history of the studied plutons. *In situ* crystal fractionation is evident during the crystallization of both the Strontian and Rogart plutons, and a late mixing event with mafic

magma can be identified in Strontian, which is not evident from whole-rock data.

(2) Other petrogenetic events, such as metasediment assimilation recorded in whole-rock isotope systematics, are not visible in the mineral chemical data presented here (trace elements). This may be a matter of timing, with *in situ* crystallization of the accessory minerals post-dating crustal assimilation that occurred during magma transport.

(3) Many elements within apatite and titanite (e.g. Sr, V, REE) closely reflect whole-rock chemistry and the degree of differentiation of the samples.

(4) All the accessory phases studied here can be dated by U–Pb methods and therefore, the association of U–Pb dating and trace element analysis could provide important additional constraints for provenance studies (e.g. McAteer *et al.*, 2010). Although tonalite–trondhjemite–granodiorite are the main plutonic rock types generated during the Archean, an important change around 2·7 Ga led to the genesis of sanukitoids. This event is often interpreted as the result of a change from shallow to steep subduction and would represent the onset of modern plate tectonics. Ultimately, the study of accessory minerals within sanukitoid-like rocks has implications for the recognition of the sanukitoid signature through time. Further work on sanukitoid accessory phases is now needed to confirm that these also reflect their original magma compositions. If successful, this will be helpful in defining the temporal distribution of sanukitoids from the detrital record.

(5) Elemental variations within zircon crystals are not petrogenetically informative.

SUPPLEMENTARY DATA

Supplementary data for this paper are available at *Journal of Petrology* online.

REFERENCES

Atherton, M. P. & Ghani, A. A. (2002). Slab breakoff: a model for Caledonian, Late Granite syn-collisional magmatism in the ortho-tectonic (metamorphic) zone of Scotland and Donegal, Ireland. *Lithos* **62**, 65–85.

Bailey, E. B. & Maufe, H. B. (1916). *The geology of Ben Nevis and Glen Coe and the surrounding country, 1st edn. Memoir of the Geological Survey of Great Britain, Sheet 53 (Scotland)*. HMSO.

Ballard, J. R., Palin, J. M. & Campbell, I. H. (2002). Relative oxidation states of magmas inferred from Ce(IV)/Ce(III) in zircon: application to porphyry copper deposits of northern Chile. *Contributions to Mineralogy and Petrology* **144**, 347–364.

Barrie, C. T. (1995). Zircon thermometry of high-temperature rhyolites near volcanic-associated massive sulfide deposits, Abitibi Subprovince, Canada. *Geology* **23**, 169–172.

Belousova, E. A., Walters, S., Griffin, W. L. & O'Reilly, S. Y. (2001). Trace-element signatures of apatites in granitoids from the Mt Isa Inlier, northwestern Queensland. *Australian Journal of Earth Sciences* **48**, 603–619.

Belousova, E. A., Griffin, W. L., O'Reilly, S. Y. & Fisher, N. I. (2002a). Apatite as an indicator mineral for mineral exploration: trace-element compositions and their relationship to host rock type. *Journal of Geochemical Exploration* **76**, 45–69.

Belousova, E. A., Griffin, W. L., O'Reilly, S. Y. & Fisher, N. I. (2002b). Igneous zircon: trace element composition as an indicator of source rock type. *Contributions to Mineralogy and Petrology* **143**, 602–622.

Brown, P. E., Miller, J. A. & Grasty, R. L. (1968). Isotopic ages of Late Caledonian granitic intrusions in the British Isles. *Proceedings of the Yorkshire Geological Society* **36**, 251–276.

Brown, P. E., Ryan, P. D., Soper, N. J. & Woodcock, N. H. (2008). The Newer Granite problem revisited: a transtensional origin for the Early Devonian Trans-Suture Suite. *Geological Magazine* **145**, 235–256.

Burnham, A. D. & Berry, A. J. (2012). An experimental study of trace element partitioning between zircon and melt as a function of oxygen fugacity. *Geochimica et Cosmochimica Acta* **95**, 196–212.

Chu, M. F., Wang, K. L., Griffin, W. L., Chung, S. L., O'Reilly, S. Y., Pearson, N. J. & Iizuka, Y. (2009). Apatite composition: tracing petrogenetic processes in Transhimalayan granitoids. *Journal of Petrology* **50**, 1829–1855.

Compston, W., Williams, I. S. & Meyer, C. (1984). U–Pb geochronology of zircons from lunar breccia 73217 using a sensitive high mass-resolution ion microprobe. *Journal of Geophysical Research—Solid Earth and Planets* **89**, B252–B534.

Dhuime, B., Hawkesworth, C. J., Cawood, P. A. & Storey, C. D. (2012). A change in the geodynamics of continental growth 3 billion years ago. *Science* **335**, 1334–1336.

Fedo, C. M. (2000). Setting and origin for problematic rocks from the >3·7 Ga Isua Greenstone Belt, southern west Greenland: Earth's oldest coarse elastic sediments. *Precambrian Research* **101**, 69–78.

Feng, R., Machado, N. & Ludden, J. (1993). Lead geochronology of zircon by laserprobe-inductively coupled plasma-mass spectrometry (LP-ICPMS). *Geochimica et Cosmochimica Acta* **57**, 3479–3486.

Ferry, J. M. & Watson, E. B. (2007). New thermodynamic models and revised calibrations for the Ti-in-zircon and Zr-in-rutile thermometers. *Contributions to Mineralogy and Petrology* **154**, 429–437.

Fowler, M. B. (1988). Ach'uaine hybrid appinite pipes: evidence for mantle-derived shoshonitic parent magmas in Caledonian granite gneiss. *Geology* **16**, 1026–1030.

Fowler, M. & Rollinson, H. (2012). Phanerozoic sanukitoids from Caledonian Scotland: Implications for Archean subduction. *Geology* **40**, 1079–1082.

Fowler, M. B., Henney, P. J., Darbyshire, D. P. F. & Greenwood, P. B. (2001). Petrogenesis of high Ba–Sr granites: the Rogart pluton, Sutherland. *Journal of the Geological Society* **158**, 521–534.

Fowler, M. B., Kocks, H., Darbyshire, D. P. F. & Greenwood, P. B. (2008). Petrogenesis of high Ba–Sr plutons from the Northern Highlands Terrane of the British Caledonian Province. *Lithos* **105**, 129–148.

Fu, B., Page, F. Z., Cavosie, A. J., Fournelle, J., Kita, N. T., Lackey, J. S., Wilde, S. A. & Valley, J. W. (2008). Ti-in-zircon thermometry: applications and limitations. *Contributions to Mineralogy and Petrology* **156**, 197–215.

Gagnevin, D., Daly, J. S. & Kronz, A. (2010). Zircon texture and chemical composition as a guide to magmatic processes and mixing in a granitic environment and coeval volcanic system. *Contributions to Mineralogy and Petrology* **159**, 579–596.

Green, T. H. & Pearson, N. J. (1986). Ti-Rich Accessory Phase Saturation in Hydrous Mafic-Felsic Compositions at High P,T. *Chemical Geology* **54**, 185–201.

Harrison, T. M. & Watson, E. B. (1984). The Behavior of Apatite during Crustal Anatexis – Equilibrium and Kinetic Considerations. *Geochimica et Cosmochimica Acta* **48**, 1467–1477.

Harrison, T. M., Watson, E. B. & Aikman, A. B. (2007). Temperature spectra of zircon crystallization in plutonic rocks. *Geology* **35**, 635–638.

Hawkesworth, C. J. & Kemp, A. I. S. (2006). Using hafnium and oxygen isotopes in zircons to unravel the record of crustal evolution. *Chemical Geology* **226**, 144–162.

Hayden, L. A. & Watson, E. B. (2007). Rutile saturation in hydrous siliceous melts and its bearing on Ti-thermometry of quartz and zircon. *Earth and Planetary Science Letters* **258**, 561–568.

Hayden, L. A., Watson, E. B. & Wark, D. A. (2008). A thermobarometer for sphene (titanite). *Contributions to Mineralogy and Petrology* **155**, 529–540.

Heaman, L. M., Bowins, R. & Crocket, J. (1990). The chemical composition of igneous zircon suites—implications for geochemical tracer studies. *Geochimica et Cosmochimica Acta* **54**, 1597–1607.

Horie, K., Hidaka, H. & Gauthier-Lafaye, F. (2008). Elemental distribution in apatite, titanite and zircon during hydrothermal alteration: Durability of immobilization mineral phases for actinides. *Physics and Chemistry of the Earth* **33**, 962–968.

Hoskin, P. W. O., Kinny, P. D., Wyborn, D. & Chappell, B. W. (2000). Identifying accessory mineral saturation during differentiation in granitoid magmas: an integrated approach. *Journal of Petrology* **41**, 1365–1396.

Hoskin, P. W. O. & Schaltegger, U. (2003). The composition of zircon and igneous and metamorphic petrogenesis. In: Hanchar, J. M. & Hoskin, P. W. O. (eds) *Zircon. Mineralogical Society of America and Geochemical Society, Reviews in Mineralogy and Geochemistry* **53**, 27–62.

Jennings, E. S., Marschall, H. R., Hawkesworth, C. J. & Storey, C. D. (2011). Characterization of magma from inclusions in zircon: Apatite and biotite work well, feldspar less so. *Geology* **39**, 863–866.

Kocks, H., Strachan, R. A., Evans, J. A. & Fowler, M. B. (2013). Contrasting magma emplacement mechanism within Rogart igneous complex, NW Scotland, record the switch from regional contraction to strike-slip during Caledonian orogeny. *Geological Magazine.* http://dx.doi.org/10.1017/S0016756813000940.

Kosler, J. & Sylvester, P. J. (2003). Present trends and the future of zircon in geochronology: Laser ablation ICPMS. In: Hanchar, J. M. & Hoskin, P. W. O. (eds) *Zircon. Mineralogical Society of America and Geochemical Society, Reviews in Mineralogy and Geochemistry* **53**, 243–275.

Larsen, L. H. (1973). Measurement of solubility of zircon (ZrSiO$_4$) in synthetic granitic melts. *Transactions of the American Geophysical Union* **54**, 479–&.

Luhr, J. F., Carmichael, I. S. E. & Varekamp, J. C. (1984). The 1982 eruptions of El Chichon volcano, Chiapas, Mexico–mineralogy and petrology of the anhydrite-bearing pumices. *Journal of Volcanology and Geothermal Research* **23**, 69–108.

Marks, M. A. W., Wenzel, T., Whitehouse, M. J., Loose, M., Zack, T., Barth, M., Worgard, L., Krasz, V., Eby, G. N., Stosnach, H. & Markl, G. (2012). The volatile inventory (F, Cl, Br, S, C) of magmatic apatite: An integrated analytical approach. *Chemical Geology* **291**, 241–255.

Martin, H., Moyen, J.-F. & Rapp, R. (2009). The sanukitoid series: Magmatism at the Archaean–Proterozoic transition. *Transactions of the Royal Society of Edinburgh* **100**, 15–33.

McAteer, C. A., Daly, J. S., Flowerdew, M. J., Connelly, J. N., Housh, T. B. & Whitehouse, M. J. (2010). Detrital zircon, detrital titanite and igneous clast U–Pb geochronology and basement–cover relationships of the Colonsay Group, SW Scotland: Laurentian provenance and correlation with the Neoproterozoic Dalradian Supergroup. *Precambrian Research* **181**, 21–42.

McDonough, W. F. & Sun, S. S. (1995). The composition of the Earth. *Chemical Geology* **120**, 223–253.

McLeod, G. W., Dempster, T. J. & Faithfull, J. W. (2011). Deciphering magma-mixing processes using zoned titanite from the Ross of Mull Granite, Scotland. *Journal of Petrology* **52**, 55–82.

Miles, A. J., Graham, C. M., Hawkesworth, C. J., Gillespie, M. R. & Hinton, R. W. (2013). Evidence for distinct stages of magma history recorded by the compositions of accessory apatite and zircon. *Contributions to Mineralogy and Petrology* **166**, 1–19.

Miller, C. F., McDowell, S. M. & Mapes, R. W. (2003). Hot and cold granites? Implications of zircon saturation temperatures and preservation of inheritance. *Geology* **31**, 529–532.

Murphy, J. B. (2013). Appinite suites: A record of the role of water in the genesis, transport, emplacement and crystallization of magma. *Earth-Science Reviews* **119**, 35–59.

Paterson, B. A. & Stephens, W. E. (1992). Kinetically induced compositional zoning in titanite—implications for accessory-phase/melt partitioning of trace elements. *Contributions to Mineralogy and Petrology* **109**, 373–385.

Paterson, B. A., Stephens, W. E. & Herd, D. A. (1989). Zoning in granitoid accessory minerals as revealed by backscattered electron imagery. *Mineralogical Magazine* **53**, 55–61.

Pearce, N. J. G., Perkins, W. T., Westgate, J. A., Gorton, M. P., Jackson, S. E., Neal, C. R. & Chenery, S. P. (1997). A compilation of new and published major and trace element data for NIST SRM 610 and NIST SRM 612 glass reference materials. *Geostandards Newsletter* **21**, 115–144.

Piccoli, P., Candela, P. & Rivers, M. (2000). Interpreting magmatic processes from accessory phases: titanite—a small-scale recorder of large-scale processes. *Transactions of the Royal Society of Edinburgh, Earth Sciences* **91**, 257–267.

Prowatke, S. & Klemme, S. (2005). Effect of melt composition on the partitioning of trace elements between titanite and silicate melt. *Geochimica et Cosmochimica Acta* **69**, 695–709.

Prowatke, S. & Klemme, S. (2006). Trace element partitioning between apatite and silicate melts. *Geochimica et Cosmochimica Acta* **70**, 4513–4527.

Rock, N.M.S. (1984). Nature and origin of calc-alkaline lamprophyre: minettes, vogesites, kersantites and spessartites. *Transactions of the Royal Society of Edinburgh, Earth Sciences* **74**, 193–227.

Rogers, G. & Dunning, G. R. (1991). Geochronology of appinitic and related granitic magmatism in the W Highlands of Scotland: constraints on the timing of transcurrent fault movement. *Journal of the Geological Society, London* **148**, 17–27.

Sabine, P. A. (1963). The Strontian granite complex, Argyllshire. *Bulletin of the Geological Survey of Great Britain* **20**, 6–42.

Sha, L. K. & Chappell, B. W. (1999). Apatite chemical composition, determined by electron microprobe and laser-ablation inductively coupled plasma mass spectrometry, as a probe into granite petrogenesis. *Geochimica et Cosmochimica Acta* **63**, 3861–3881.

Smith, M. P., Storey, C. D., Jeffries, T. E. & Ryan, C. (2009). *In situ* U–Pb and trace element analysis of accessory minerals in the Kiruna district, Norrbotten, Sweden: new constraints on the timing and origin of mineralization. *Journal of Petrology* **50**, 2063–2094.

Soper, N. J. (1963). The structure of the Rogart igneous complex, Sutherland, Scotland. *Quarterly Journal of the Geological Society of London* **119**, 445–478.

Soper, N. J. (1986). The Newer Granite problem—a geotectonic view. *Geological Magazine* **123**, 227–236.

Soper, N. J., England, R. W., Snyder, D. B. & Ryan, P. D. (1992). The Iapetus suture zone in England, Scotland and eastern Ireland—a reconciliation of geological and deep seismic data. *Journal of the Geological Society, London* **149**, 697–700.

Stephens, W.E. & Halliday, A.N. (1984). Geochemical contrasts between late Caledonian granitoid pluton and morthern, central and southern Scotland. *Transactions of the Royal Society of Edinburgh, Earth Sciences* **75**, 259–273.

Stephenson, D., Bevins, R. E., Millward, D., Highton, A. J., Parsons, I., Stone, P. & Wadsworth, W. J. (1999). Caledonian igneous rocks of Great Britain. *Geological Conservation Review Series* **17**, 648.

Tarney, J. & Jones, C. E. (1994). Trace element geochemistry of orogenic igneous rocks and crustal growth models. *Journal of the Geological Society, London* **151**, 855–868.

Tepper, J. H. & Kuehner, S. M. (1999). Complex zoning in apatite from the Idaho batholith: A record of magma mixing and intracrystalline trace element diffusion. *American Mineralogist* **84**, 581–595.

Tiepolo, M., Oberti, R. & Vannucci, R. (2002). Trace-element incorporation in titanite: constraints from experimentally determined solid/liquid partition coefficients. *Chemical Geology* **191**, 105–119.

Tyler, I. M. & Ashworth, J. R. (1983). The metamorphic environment of the Foyers Granitic Complex. *Scottish Journal of Geology* **19**, 271–285.

Trail, D., Watson, E. B. & Tailby, N. D. (2011). The oxidation state of Hadean magmas and implications for early Earth's atmosphere. *Nature* **480**, 79–83.

Watson, E. B. (1979). Zircon saturation in felsic liquids—experimental results and applications to trace-element geochemistry. *Contributions to Mineralogy and Petrology* **70**, 407–419.

Watson, E. B. & Harrison, T. M. (1983). Zircon saturation revisited—temperature and composition effects in a variety of crustal magma types. *Earth and Planetary Science Letters* **64**, 295–304.

Watson, E. B. & Liang, Y. (1995). A simple model for sector zoning in slowly grown crystals: Implications for growth rate and lattice diffusion, with emphasis on accessory minerals in crustal rocks. *American Mineralogist* **80**, 1179–1187.

Wiedenbeck, M., Hanchar, J. M., Peck, W. H. *et al.* (2004). Further characterisation of the 91500 zircon crystal. *Geostandards and Geoanalytical Research* **28**, 9–39.

Whitney, D. L. & Evans, B. W. (2010). Abbreviations for names of rock-forming minerals. *American Mineralogist* **95**, 185–187.